

---

# Text Has Curvature

---

Karish Grover<sup>1,2</sup> Hanqing Zeng<sup>2</sup> Yinglong Xia<sup>2</sup> Christos Faloutsos<sup>1</sup> Geoffrey J. Gordon<sup>1</sup>

## Abstract

Does text have an intrinsic curvature? Language is increasingly modeled in curved geometries—hyperbolic spaces for hierarchy, mixed-curvature manifolds for compositional structure—yet a basic scientific question remains unresolved: *what does curvature mean for text itself*, in a way that is native to language rather than an artifact of the embedding space we choose? We argue that text does indeed have curvature, and show how to *detect* it, *define* it, and *use* it. To this end, we propose **Texture**, a text-native, word-level discrete curvature signal, and make three contributions. **(a) Existence:** We provide empirical and theoretical certificates that semantic inference in natural corpora is non-flat, i.e. language has inherent curvature. **(b) Definition:** We define Texture by reconciling left- and right-context beliefs around a masked word through a Schrödinger bridge, yielding a curvature field that is positive where context *focuses* meaning and negative where it *fans out* into competing continuations. **(c) Utility:** Texture is actionable: it serves as a general-purpose measurement and control primitive enabling *geometry without geometric training*; we instantiate it on two representative tasks, improving long-context inference through curvature-guided compression and retrieval-augmented generation through curvature-guided routing. Together, our results establish a text-native curvature paradigm, making curvature measurable and practically useful.

## 1. Introduction

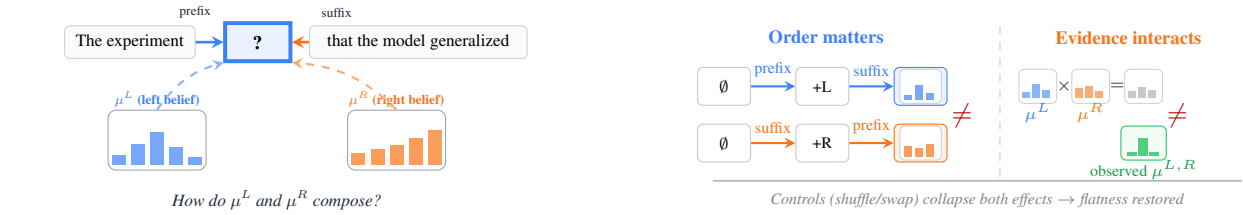
Language is not merely a bag of words: it expresses hierarchies (taxonomies, entailment chains), multi-way relations (entities, events, discourse structure), and nonlocal constraints (agreement, coreference, long-range dependencies). A growing body of work has therefore advocated

<sup>1</sup>Carnegie Mellon University <sup>2</sup>Meta. Correspondence to: Karish Grover <karishg@cs.cmu.edu>.

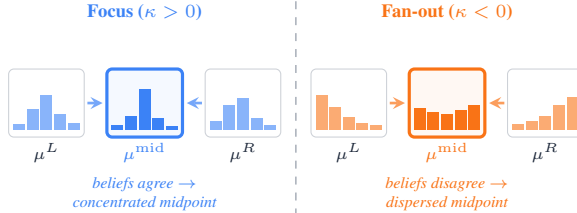
*non-Euclidean* geometric foundations for language representations, including hyperbolic and mixed-curvature modeling (Nickel & Kiela, 2017; Gu et al., 2018). Recent proposals even train large language models directly in hyperbolic spaces or with curvature-mixture architectures, motivated by the claim that text has inherent curved structure (He et al., 2025; Chen et al., 2024). However, these efforts largely treat curvature as an *architectural or embedding choice* rather than a *text-native quantity*. This leaves a foundational gap: *before we train curvature-aware models, how do we know what the curvature of text is?*

**The gap: no text-native curvature formalism.** For graphs, intrinsic notions of discrete curvature are well developed. Ollivier–Ricci curvature defines curvature locally at each edge by comparing optimal-transport distances to combinatorial distances (Ollivier, 2007); it has been applied to detect communities, identify bottlenecks, and improve message-passing in GNNs (Sia et al., 2019). **No analogous formalism exists for text.** Current geometric approaches to language embed tokens or sequences onto a curved manifold and validate the choice by downstream performance (Ganea et al., 2018; Gu et al., 2018; Grover et al., 2025). The assumption that text “has curvature” is never formalized, tested, or defined—curvature remains an architectural prior rather than a measurable property.

**Our approach: curvature as a property of two-sided inference.** We propose that if curvature is intrinsic to language, it should be detectable *before* committing to a curved architecture. The natural locus is the *word-in-context slot*: a position  $i$  where both prefix  $x_{<i}$  and suffix  $x_{>i}$  constrain what can appear. A prefix suggests plausible continuations; a suffix retroactively constrains what could have occurred. The scientific object is *two-sided inference*—how these two sources of evidence interact when they inform the same latent slot meaning. Rather than embedding tokens in a chosen manifold, we represent each context side as a *belief distribution* over a finite set of plausible slot states, extracted from a frozen language model. Curvature then describes how these beliefs *compose*: do they reconcile into a single semantic basin (*focus*), or do they sustain competing alternatives (*fan-out*)? This framing yields a measurable, signed curvature field over positions in a sequence. We develop this idea in three stages:



(a) **The word-in-context slot (local object).** A prefix and a suffix each induce a belief distribution over plausible slot fillers ( $\mu^L, \mu^R$ ). Text curvature, in our view, is about *how two-sided evidence composes* at this local slot.



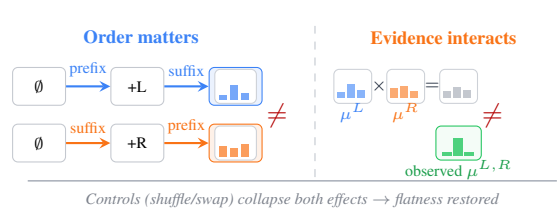
(c) **Texture: signed curvature from reconciliation.** Texture reconciles  $\mu^L$  and  $\mu^R$  via a neutral midpoint  $\mu^{\text{mid}}$ : concentrated reconciliation yields *focus* ( $\kappa > 0$ ); dispersed reconciliation yields *fan-out* ( $\kappa < 0$ ). Details in Section 5.

*Figure 1. Texture overview.* (a) Our primitive object is a two-sided slot with prefix/suffix beliefs (order-sensitivity and evidence interaction), motivating curvature and enabling definition-independent existence tests (Section 4). (c) Texture defines a text-native signed curvature by comparing endpoints to a conservative symmetric reconciliation (Section 5). (d) The resulting curvature field is a general-purpose control signal: we instantiate it on pruning and retrieval, but it applies broadly to language tasks requiring context-aware resource allocation (Section 6).

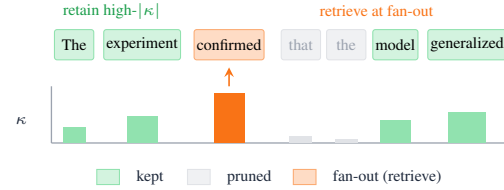
**(a) Existence** (Section 4). Before defining curvature, we ask: *is two-sided inference over natural text effectively flat?* Flatness makes falsifiable predictions about how left and right evidence should compose as context expands. We instantiate two classical primitives—holonomy, a path-order independence condition from differential geometry (Ni, 2024), and product-of-experts combination (Hinton, 1999)—as *flatness nulls* (null hypotheses that hold if text were geometrically flat) for two-sided text inference, and test them on natural corpora against matched coherence-destroying controls. Natural text systematically violates both nulls; controls restore near-flat behavior. This establishes that non-flat structure is real and intrinsic, not a definitional artifact.

**(b) Definition** (Section 5). Having established non-flat behavior, we introduce *Texture*: a text-native curvature primitive that assigns each slot a signed scalar  $\kappa_i$ . Given boundary beliefs ( $\mu_i^L, \mu_i^R$ ) and a neutral semantic-drift kernel, we compute the Schrödinger-bridge midpoint—the least-deforming reconciliation in KL—and measure whether this midpoint concentrates free energy (*focus*,  $\kappa_i > 0$ ) or disperses it (*fan-out*,  $\kappa_i < 0$ ) (Léonard, 2013; Cuturi, 2013). The definition is well-posed on finite supports, making it practical rather than architectural.

**(c) Utility** (Section 6). Finally, we show that the curvature



(b) **Flatness fails in two-sided inference.** *Left:* final belief depends on context order. *Right:* two-sided belief  $\neq$  additive combination. These failures motivate curvature and underpin our existence tests (Section 4); matched controls collapse both effects.



(d) **Curvature as control.** CURVPRUNE retains high-curvature spans under a token budget; CURVFLAG triggers retrieval at fan-out pivots. Both enable geometry-aware context management without training a curved generator (Section 6).

field is actionable: because Texture can be evaluated on any frozen model, it provides a control signal for inference-time resource allocation. We introduce two plug-in utilities: CURVPRUNE, which allocates a fixed prompt budget toward high-curvature spans, and CURVFLAG, which triggers retrieval at fan-out pivots where local context is insufficient (Jiang et al., 2023a; Lewis et al., 2020). Both utilities require no geometric training: curvature is estimated by a small frozen model, while the downstream generator can be any black-box LLM. This positions Texture as a practical alternative to training curved LLMs—we exploit curved structure by *measuring* it rather than *learning* it.

## Contributions.

1. To the best of our knowledge, this is the first work to define, measure, and operationalize an intrinsic notion of curvature for natural language text.
2. **Existence.** We provide definition-independent certificates that two-sided semantic inference over natural text is non-flat, using two complementary flatness nulls—holonomy commutativity and product-of-experts additivity (CEI)—with matched coherence-destroying controls and an empirical falsification protocol.
3. **Definition.** We introduce *Texture*, a text-native curva-

ture primitive that reconciles left- and right-context beliefs via a Schrödinger bridge, yielding an interpretable signed field: positive where context focuses meaning, negative where it fans out into competing alternatives.

4. **Utility.** We demonstrate that Texture is actionable as a control signal, introducing training-free methods for curvature-guided prompt compression and retrieval routing that improve long-context inference.

## 2. Related Work

**Curved representations for language and foundation models.** A growing line of work argues that language exhibits hierarchical and scale-free structure that can be modeled more naturally in non-Euclidean spaces. This view is synthesized in the recent position paper of He et al. (2025). On the modeling side, hyperbolic geometry has been explored from embedding-level approaches to end-to-end hyperbolic networks (Nickel & Kiela, 2017; Ganea et al., 2018), and Chen et al. (2024) train a hyperbolic pre-trained language model with broad gains over Euclidean baselines. These efforts validate curvature as an *architectural prior*; our work targets a different primitive: a *text-native* curvature defined and measured locally from two-sided inference without committing the generator to a curved manifold.

**Discrete curvature on graphs.** Outside NLP, a substantial literature has developed discrete curvature notions for graphs and networks. Ollivier-Ricci curvature (ORC) defines curvature via optimal-transport contraction of neighborhood measures under a random walk (Ollivier, 2007), and Forman introduced a combinatorial Ricci curvature for cell complexes (Forman, 2003), later adapted to weighted networks as an efficient edge-based curvature statistic (Sreejith et al., 2016). These notions quantify curvature of an *explicit discrete space* (graph/Markov structure) chosen by the practitioner. In language one can build auxiliary graphs (co-occurrence, syntactic, knowledge graphs), but this does not define curvature of *text itself* at the word-in-context level. Our contribution fills this gap by defining curvature directly on the *two-sided belief geometry* at a slot, rather than on a user-chosen graph.

**Entropic transport and Schrödinger bridges as a reconciliation primitive.** Entropic optimal transport provides stable, scalable computation via Sinkhorn-type scaling (Cuturi, 2013), and Schrödinger bridges define entropic interpolations by KL projection onto reference Markov paths (Léonard, 2013). These tools have also been used to study entropic curvature on discrete spaces via behavior of entropy along Schrödinger bridges (Samson, 2022). We repurpose this machinery for language: the bridge midpoint becomes a symmetry-respecting reconciliation of prefix and suffix

beliefs, and Texture reads curvature from whether reconciliation *focuses* meaning or *fans out*.

**Long-context efficiency: compression, retrieval, and adaptive routing.** Long-context deployment motivates methods that allocate limited compute and context budget selectively. Prompt compression methods reduce cost under a token budget (Jiang et al., 2023a), while retrieval-augmented generation injects external evidence for knowledge-intensive tasks (Lewis et al., 2020). These pipelines propose heuristics or learned controllers, but do not provide a text-native geometric diagnostic of when two-sided evidence is redundant versus underdetermined. Our utilities use curvature as a signal for pruning and retrieval, leaving the generator unchanged.

## 3. Preliminaries

We collect notation and standard probabilistic/transport primitives used throughout. All paper-specific operators (e.g., *Texture* curvature) are defined later; here we only define the shared objects they are built from.

**Text, slots, and context radii.** We write a token sequence as  $x_{1:n} = (x_1, \dots, x_n)$ . For index  $i$ , denote prefix  $x_{<i} := x_{1:i-1}$  and suffix  $x_{>i} := x_{i+1:n}$ . For radii  $L, R \in \mathbb{N}$ , we use truncated contexts  $x_{<i}^L := x_{i-L:i-1}$  and  $x_{>i}^R := x_{i+1:i+R}$  (clipped at boundaries), and the contextual slot  $(x_{<i}^L, \square, x_{>i}^R)$  where  $\square$  marks a missing filler.

**Finite slot state spaces, tail bucket, and belief extractors.** All core objects live on a *finite* slot-local state space  $\mathcal{S}_i$  and its simplex  $\Delta(\mathcal{S}_i) := \{\mu \in \mathbb{R}_{\geq 0}^{\mathcal{S}_i} : \sum_{s \in \mathcal{S}_i} \mu(s) = 1\}$ . We use one-sided boundary beliefs  $\mu_i^L, \mu_i^R \in \Delta(\mathcal{S}_i)$  (prefix-only vs. suffix-only) and a two-sided belief extractor  $\mathcal{B}_{\leftrightarrow}$  (e.g., a masked/infilling LM (Devlin et al., 2019)). On a context-radius grid, the two-sided posterior field is written  $\mu_i(L, R) := \mathcal{B}_{\leftrightarrow}(\cdot \mid x_{<i}^L, \square, x_{>i}^R; \mathcal{S}_i) \in \Delta(\mathcal{S}_i)$ . Because practical extractors return truncated supports (e.g., top- $k$  candidates), we use a *canonical per-slot support* with an explicit tail bucket to avoid support-change artifacts: for any belief  $\mu$  on a larger ambient domain, let  $\text{TopK}(\mu)$  be its  $k$  highest-probability states (ties broken deterministically), define  $\mathcal{C}_i := \text{TopK}(\mu_i^L) \cup \text{TopK}(\mu_i^R)$  and  $\mathcal{S}_i := \mathcal{C}_i \cup \{\text{tail}\}$ , and push residual mass to tail via  $\mu(\text{tail}) := 1 - \sum_{s \in \mathcal{C}_i} \mu(s)$ , leaving  $\mu(s)$  unchanged for  $s \in \mathcal{C}_i$ . We apply this map to each boundary belief and each  $\mu_i(L, R)$  so that all objects share a fixed domain.

**KL divergence.** For  $\mu, \nu \in \Delta(\mathcal{S})$  with  $\mu \ll \nu$ , the Kullback–Leibler divergence is  $\text{KL}(\mu \parallel \nu) := \sum_{s \in \mathcal{S}} \mu(s) \log \frac{\mu(s)}{\nu(s)}$ . KL is used both as a discrepancy between beliefs (e.g., CEI in Section 4) and as the objective defining Schrödinger bridges (Section 5).

**Markov kernels, stationarity, and reversibility.** A Markov kernel on a finite  $\mathcal{S}$  is a row-stochastic matrix  $K$ ; it pushes forward beliefs by  $(\mu K)(s') = \sum_s \mu(s)K(s, s')$ . A distribution  $\pi$  is stationary if  $\pi = \pi K$ . We call  $K$  reversible w.r.t.  $\pi$  if it satisfies detailed balance:  $\pi(s)K(s, s') = \pi(s')K(s', s)$  for all  $s, s'$ . Reversibility ensures the neutral reference dynamics in Texture are left-right invariant.

**Schrödinger bridges and Sinkhorn scaling on finite supports.** Fix a reversible reference chain with stationary  $\pi$  and kernel  $K$  on  $\mathcal{S}$ . For endpoint beliefs  $\mu_0, \mu_2 \in \Delta(\mathcal{S})$ , we use the minimal two-step reference path measure  $R(s_0, s_1, s_2) := \pi(s_0)K(s_0, s_1)K(s_1, s_2)$  and define the two-step Schrödinger bridge as the entropic projection  $P^* \in \arg \min_{P: P_0=\mu_0, P_2=\mu_2} \text{KL}(P\|R)$ . On finite spaces with strictly positive kernels,  $P^*$  exists, is unique, and admits a multiplicative scaling form  $P^*(s_0, s_1, s_2) = u(s_0)v(s_2)R(s_0, s_1, s_2)$  for endpoint potentials  $(u, v)$  chosen to match the marginals. Solving for  $(u, v)$  reduces to a matrix-scaling / iterative proportional fitting problem (Sinkhorn–Knopp) and can be computed efficiently by Sinkhorn iterations (Cuturi, 2013). The midpoint  $(P^*)_1$  provides a canonical, symmetric reconciliation between endpoints and is the primitive used in Section 5.

## 4. Existence: Curvature Fingerprints in Two-Sided Inference Geometry

Can we certify that natural text exhibits *non-flat* two-sided inference geometry *without* committing to any particular curvature definition? Part I answers this by proposing two *definition-independent*, falsifiable flatness nulls on the two-sided posterior field. Violations of either null are curvature certificates: they witness genuine left-right interaction in contextual belief composition. We present the nulls and their informal equivalences in the main text, with full statements and proofs in Appendix C, and we empirically falsify both nulls with coherence-destroying controls in §4.3.

### 4.1. Two-Sided Posterior Field

Fix a token sequence  $x_{1:n}$  and an index  $i$ . For radii  $L, R \in \mathbb{N}$ , let  $x_{<i}^L := x_{i-L:i-1}$  and  $x_{>i}^R := x_{i+1:i+R}$  denote truncated left and right contexts (clipped at boundaries), and consider the slot  $(x_{<i}^L, \square, x_{>i}^R)$ . Let  $\mathcal{S}_i$  be a finite slot-local state space (e.g., top- $k$  candidates plus a tail bucket as in §3). Given a two-sided belief extractor  $\mathcal{B}_{\leftrightarrow}$  (e.g., an infilling model), define the posterior field

$$\mu_i(L, R) := \mathcal{B}_{\leftrightarrow}(\cdot \mid x_{<i}^L, \square, x_{>i}^R ; \mathcal{S}_i) \in \Delta(\mathcal{S}_i). \quad (1)$$

The theory in Appendix C assumes full support, which in practice is ensured by the tail bucket and/or a small  $\varepsilon$ -smoothing.

### 4.2. Falsifiable Flatness Nulls and Curvature Certificates

Curvature is a second-order phenomenon: in a flat geometry, incremental evidence updates should compose in a path-independent way. We formalize this intuition as two complementary, falsifiable flatness nulls on  $(L, R) \mapsto \mu_i(L, R)$ .

**Certificate I: Holonomy (order-sensitive evidence updates).** Fix a reference state  $s_{\text{ref}} \in \mathcal{S}_i$  and define log-odds coordinates

$$u_{i,s}(L, R) := \log \frac{\mu_i(L, R)(s)}{\mu_i(L, R)(s_{\text{ref}})}, \quad s \in \mathcal{S}_i. \quad (2)$$

Define the unit-square holonomy

$$\Omega_{i,s}(L, R) := u_{i,s}(L+1, R+1) - u_{i,s}(L+1, R) - u_{i,s}(L, R+1) + u_{i,s}(L, R), \quad (3)$$

which measures whether the one-step gain from extending  $R$  depends on whether  $L$  has already been extended (and vice versa). In a flat (path-independent) regime, such incremental updates commute and  $\Omega_{i,s}$  vanishes.

**Theorem 4.1** (Holonomy flatness null; see Theorem C.1). *Assume  $\mu_i(L, R) \in \Delta^{\circ}(\mathcal{S}_i)$  on a rectangular grid domain. Then  $\Omega_{i,s}(L, R) \equiv 0$  for all  $s$  and all unit squares if and only if there exist functions  $\alpha_{i,s}(\cdot)$  and  $\beta_{i,s}(\cdot)$  such that  $u_{i,s}(L, R) = u_{i,s}(0, 0) + \alpha_{i,s}(L) + \beta_{i,s}(R)$ . Equivalently, left and right evidence contribute additively in log-odds.*

**Curvature certificate (Holonomy).** If  $\Omega_{i,s}(L, R) \neq 0$  for some  $s$  and adjacent cell  $(L, R)$ , then the additive-separability flatness null fails. We summarize holonomy per slot by an RMS magnitude over a small grid  $\mathcal{G}$  (and optionally probability weights; see Appendix C.1):

$$h_i := \left( \frac{1}{|\mathcal{G}|} \sum_{(L,R) \in \mathcal{G}} \sum_{s \in \mathcal{S}_i} w_{i,s}(L, R) \Omega_{i,s}(L, R)^2 \right)^{1/2}, \quad (4)$$

where  $w_{i,s}(L, R) \propto \mu_i(L+1, R+1)(s)$  (normalized over  $s$ ) emphasizes probable states (Appendix C.1).

**Certificate II: Evidence additivity (Product-of-Experts) and CEI.** A second flatness prediction is that two-sided evidence should combine additively in log space. For fixed radii  $(L, R)$ , define one-sided boundary beliefs  $\mu_i^{\leftarrow}(L) := \mu_i(L, 0)$ ,  $\mu_i^{\rightarrow}(R) := \mu_i(0, R)$ , and base belief  $\mu_i^{(0)} := \mu_i(0, 0)$ . The Product-of-Experts reconstruction is

$$\mu_i^{\text{PoE}}(L, R)(s) \propto \frac{\mu_i^{\leftarrow}(L)(s) \mu_i^{\rightarrow}(R)(s)}{\mu_i^{(0)}(s)}. \quad (5)$$

We measure deviation from this null by the Contextual Evidence Interaction statistic

$$\text{CEI}_i(L, R) := \text{KL}(\mu_i(L, R) \parallel \mu_i^{\text{PoE}}(L, R)) \geq 0. \quad (6)$$

**Theorem 4.2** (PoE flatness null; see Theorem C.2). Assume  $\mu_i(L, R) \in \Delta^\circ(\mathcal{S}_i)$ . Then  $\text{CEI}_i(L, R) = 0$  if and only if  $\mu_i(L, R) = \mu_i^{\text{PoE}}(L, R)$ . In particular, under an additive-evidence/conditional-independence null where left and right context contribute independent log Bayes factors given the slot value, PoE holds and  $\text{CEI}_i(L, R) = 0$ .

**Curvature certificate (PoE/CEI).** If  $\text{CEI}_i(L, R) > 0$ , then the additive-evidence flatness null fails, witnessing non-additive left-right interaction in two-sided inference. Holonomy probes *order-sensitivity* around loops in  $(L, R)$ , while CEI probes *non-additivity* of evidence composition. Both certificates are definition-independent: they remain meaningful regardless of how one later defines Texture.

### 4.3. Empirical Falsification on Natural Corpora

We test whether natural text violates these flatness nulls using a frozen infilling model  $\mathcal{B}_{\leftrightarrow}$  instantiated by distilroberta-base (a distilled RoBERTa model; Sanh et al., 2019; Liu et al., 2019). We evaluate 1000 randomly sampled slots per corpus on the radius grid  $L, R \in \{0, 1, 2, 4, 8\}$  using a fixed per-slot support  $\mathcal{S}_i$  (with a tail bucket; details in Appendix C.3). We compare *natural text* to two coherence-destroying controls: (i) **suffix-swap**, which exchanges the right contexts of matched slots, and (ii) **local-shuffle**, which permutes tokens within the right window while preserving its multiset. Both preserve surface statistics while disrupting two-sided coherence.

Figure 2 summarizes both certificates on WikiText-2 (Merity et al., 2016) and OpenWebText (Gokaslan & Cohen, 2019). Natural text exhibits substantially larger holonomy magnitude  $h_i$  and larger CEI than either control, refuting both commuting-update and additive-evidence nulls. Additional diagnostics (including a discrete telescoping sanity check, a scale-sensitive plot, and full numeric summaries with bootstrap CIs) appear in Appendix C.4. Together, these two falsifiable certificates establish an existence fact independent of our later definitions: two-sided inference geometry over natural text is generically non-flat. Section 5 (Definition) defines Texture to measure this interaction; Section 6 (Utility) applies the resulting curvature as a control signal.

## 5. Texture: Contextual Bridge Curvature

Section 4 established—via definition-independent, falsifiable certificates—that two-sided inference at a word-in-context slot exhibits intrinsic second-order interaction. We now define *Texture*, a text-native curvature primitive. Our methodological stance is that curvature should be defined at the smallest unit where two independent evidence axes exist: the slot  $(x_{<i}, \square, x_{>i})$ . A slot admits (i) a left belief induced by the prefix and (ii) a right belief induced by the suffix, and it is precisely at this interface that “flat” additive com-

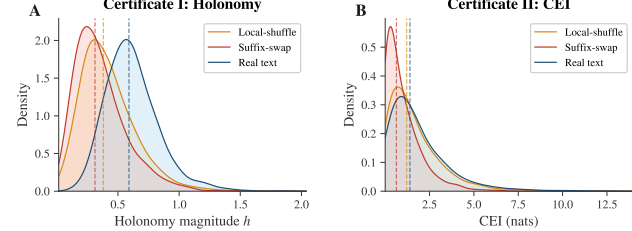


**Figure 2. Empirical falsification of flatness nulls (Panels A–B).** Distributions are over 1000 slots per corpus (WikiText-2 and OpenWebText) using distilroberta-base. **(A)** Holonomy magnitude  $h_i$  is consistently higher on natural text than on suffix-swap and local-shuffle controls, indicating order-sensitive evidence updates in two-sided inference. **(B)** CEI shows analogous separation, indicating non-additive evidence composition relative to the PoE null. Full diagnostics, medians/effect sizes, and bootstrap CIs appear in Appendix C.4.

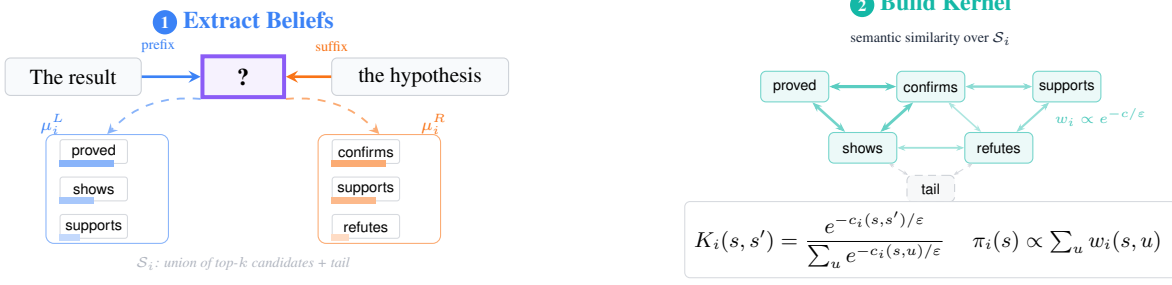
position can fail. Texture assigns each slot  $i$  a signed scalar  $\kappa_i$  with an interpretable sign: *focus* ( $\kappa_i > 0$ ), where two-sided evidence concentrates meaning into a semantic basin, and *fan-out* ( $\kappa_i < 0$ ), where evidence induces branching ambiguity among alternatives.

The definition is constrained by two design principles. First, Texture must be intrinsically *two-sided* and symmetric in left and right context. Second, the reconciliation midpoint must not be chosen heuristically; it should be uniquely determined as the KL-closest two-sided reconciliation relative to a *neutral* notion of semantic motion. We implement this principle using a finite-state two-step Schrödinger bridge midpoint (Léonard, 2013; Appendix D.2). Concretely, given boundary beliefs  $(\mu_i^L, \mu_i^R)$  on a finite state space  $\mathcal{S}_i$ , we build a reversible kernel  $K_i$  from a symmetric cost  $c_i$  and compute the bridge midpoint  $\mu_i^{\text{mid}}$ . Curvature is read from its free-energy gap.

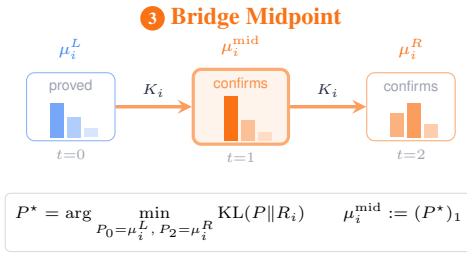
### 5.1. Slot State Space and Boundary Beliefs

Fix a token sequence  $x_{1:n}$  and a slot index  $i$ . We model the contextual blank  $(x_{<i}, \square, x_{>i})$  as two observations of an unobserved slot state  $Z_i \in \mathcal{S}_i$ , where  $\mathcal{S}_i$  is a *finite* state space local to slot  $i$ . Finiteness is a computational design choice: Texture is meant to be computed from truncated (top- $k$ ) supports produced by frozen models.

A *left boundary belief* is  $\mu_i^L \in \Delta(\mathcal{S}_i)$  intended to approximate  $P(Z_i = \cdot | x_{<i})$ , and a *right boundary belief* is  $\mu_i^R \in \Delta(\mathcal{S}_i)$  intended to approximate  $P(Z_i = \cdot | x_{>i})$ . The definition is agnostic to how these beliefs are obtained; we use simple frozen-model extractors in §7. Texture is a single operator that can be instantiated longitudinally (token-filler state spaces) or transversally (relational state spaces); we give the full relational instantiation in Appendix D.7.



(a) **Boundary beliefs (slot input).** For a slot  $(x_{<i}, \square, x_{>i})$ , a frozen belief extractor yields prefix and suffix distributions  $\mu_i^L$  and  $\mu_i^R$  over a finite candidate set  $\mathcal{S}_i$  (Top- $k$  union + tail).



(c) **Schrödinger-bridge reconciliation.** Using the reference dynamics induced by  $(\pi_i, K_i)$ , we compute the two-step Schrödinger bridge from  $\mu_i^L$  to  $\mu_i^R$ ; its midpoint marginal  $\mu_i^{\text{mid}}$  is a canonical, symmetric reconciliation of two-sided evidence.

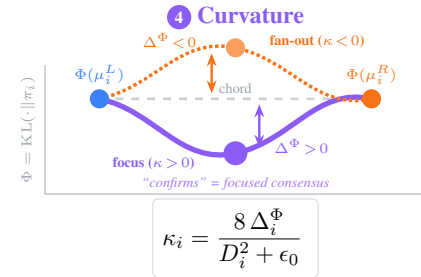
*Figure 3. Texture operator pipeline.* Given a word-in-context slot, we (a) extract boundary beliefs  $\mu_i^L, \mu_i^R$  on  $\mathcal{S}_i$ , (b) build a neutral kernel  $K_i$  from semantic costs, (c) compute the Schrödinger-bridge midpoint  $\mu_i^{\text{mid}}$  as conservative two-sided reconciliation, and (d) read off signed curvature from the midpoint's behavior (focus vs fan-out).

**Canonical support with a tail bucket.** To avoid support-mismatch artifacts from truncation, we define a canonical per-slot support by augmenting the union of top- $k$  candidates with a tail bucket state. Let  $k \in \mathbb{N}$  and let  $\text{TopK}(\mu)$  return the  $k$  highest-probability states under  $\mu$  (ties broken deterministically). Define  $\mathcal{C}_i := \text{TopK}(\mu_i^L) \cup \text{TopK}(\mu_i^R)$  and  $\mathcal{S}_i := \mathcal{C}_i \cup \{\text{tail}\}$ . We push forward beliefs to  $\mathcal{S}_i$  by assigning leftover mass to tail:  $\mu_i^L(\text{tail}) := 1 - \sum_{s \in \mathcal{C}_i} \mu_i^L(s)$  and  $\mu_i^R(\text{tail}) := 1 - \sum_{s \in \mathcal{C}_i} \mu_i^R(s)$ , while keeping  $\mu_i^L(s), \mu_i^R(s)$  unchanged for  $s \in \mathcal{C}_i$ . This avoids renormalization and ensures downstream objects are well-posed on a fixed domain.

## 5.2. Neutral Kernel and Bridge Midpoint

Texture requires a neutral reference notion of semantic motion on  $\mathcal{S}_i$ , specified by a symmetric ground cost  $c_i : \mathcal{S}_i \times \mathcal{S}_i \rightarrow \mathbb{R}_{\geq 0}$  with  $c_i(s, s') = c_i(s', s)$  and  $c_i(s, s) = 0$ . In longitudinal mode we induce  $c_i$  from frozen embeddings, e.g.  $c_i(s, s') := \|\hat{e}(s) - \hat{e}(s')\|_2^2$  with  $\hat{e}(s) := e(s)/\|e(s)\|_2$ , and in transversal mode  $c_i$  is defined on relational nodes (Appendix D.7). Fix a temperature  $\varepsilon > 0$  and define the

(b) **Neutral semantic motion kernel.** A symmetric slot-local semantic cost  $c_i$  defines affinities among candidates in  $\mathcal{S}_i$ ; row-normalization yields a Markov kernel  $K_i$  (with stationary  $\pi_i$ ) that serves as a neutral notion of “semantic drift” for reconciliation.



(d) **Signed curvature from midpoint behavior.** We compare an endpoint chord to the midpoint under a KL-based free-energy functional: midpoints below the chord indicate *focus* ( $\kappa_i > 0$ ), while midpoints above indicate *fan-out* ( $\kappa_i < 0$ ).

Gibbs affinity and row-stochastic kernel as:

$$G_i(s, s') := \exp\left(-\frac{c_i(s, s')}{\varepsilon}\right), \quad (7)$$

$$K_i(s, s') := \frac{G_i(s, s')}{\sum_{u \in \mathcal{S}_i} G_i(s, u)}.$$

Because  $G_i$  is symmetric and strictly positive,  $K_i$  is reversible with stationary distribution

$$\pi_i(s) \propto \sum_{u \in \mathcal{S}_i} G_i(s, u), \quad (8)$$

$$\pi_i(s) K_i(s, s') = \pi_i(s') K_i(s', s) \quad (\text{Appendix D.1}).$$

We use a two-step horizon  $S_0 \rightarrow S_1 \rightarrow S_2$  because it is the minimal discrete-time construction with a symmetric midpoint. Define the two-step reference path measure on  $\mathcal{S}_i^3$  by

$$R_i(s_0, s_1, s_2) := \pi_i(s_0) K_i(s_0, s_1) K_i(s_1, s_2). \quad (9)$$

Among all path measures whose endpoints match the boundary beliefs, select the KL-closest one:

$$P_i^* \in \arg \min_{P: P_0=\mu_i^L, P_2=\mu_i^R} \text{KL}(P||R_i). \quad (10)$$

Define the midpoint belief as the time-1 marginal  $\mu_i^{\text{mid}} := (P_i^*)_1$ . This midpoint is uniquely defined under mild full-support assumptions and admits an endpoint scaling/message-passing form (Appendix D.2; Cuturi, 2013).

### 5.3. From Midpoint to Curvature: Texture

Texture reads curvature from a midpoint convexity defect of a canonical free-energy functional, normalized by the bridge energy. We use the canonical choice

$$\Phi_i(\rho) := \text{KL}(\rho \parallel \pi_i), \quad \rho \in \Delta(\mathcal{S}_i). \quad (11)$$

Define the midpoint free-energy gap

$$\Delta_i^\Phi := \frac{1}{2}(\Phi_i(\mu_i^L) + \Phi_i(\mu_i^R)) - \Phi_i(\mu_i^{\text{mid}}), \quad (12)$$

and the bridge energy  $D_i^2 := \text{KL}(P_i^* \parallel R_i)$ , which can be computed from endpoint scaling potentials (Appendix D.3). Finally, with a small numerical guard  $\epsilon_0 > 0$  (used only when  $D_i^2$  is extremely small), define

$$\kappa_i := \frac{8 \Delta_i^\Phi}{D_i^2 + \epsilon_0}. \quad (13)$$

We interpret  $\Delta_i^\Phi > 0$  (hence  $\kappa_i > 0$ ) as *focus* and  $\Delta_i^\Phi < 0$  as *fan-out*. The factor 8 matches the midpoint specialization of  $\lambda$ -convexity along constant-speed geodesics; a self-contained derivation appears in Appendix D.4 (see also Ambrosio et al., 2005).

### 5.4. Computation

For each slot, the dominant computation is a small matrix-scaling (Sinkhorn/IPFP) problem on the strictly positive endpoint matrix  $R_{02}(s_0, s_2) = \pi_i(s_0)(K_i^2)(s_0, s_2)$  (Appendix D.2). In practice we ensure full support by a tiny smoothing of  $\mu_i^L, \mu_i^R$  and of the kernel when needed; the resulting midpoint, gap, and energy are stable on finite supports (Theorem D.5). An explicit step-by-step algorithmic summary is given in Appendix D.6.

## 6. Utility: Curvature as an Inference-Time Control Primitive

Sections 4–5 show that two-sided inference over natural text is empirically non-flat and can be summarized by a *signed* curvature field  $\{\kappa_i\}$  with an operational semantics:  $\kappa_i > 0$  indicates *focus* (two-sided evidence concentrates meaning), while  $\kappa_i < 0$  indicates *fan-out* (two-sided evidence disperses mass over alternatives). Here we show that the same curvature field is not merely descriptive: it can be used as a *model-agnostic inference-time control signal* for long-context systems. We develop two representative applications—budgeted prompt construction and retrieval

routing—because they isolate a common systems question: *where is local context sufficient, and where is additional evidence or budget needed?* Since Texture only requires two-sided beliefs, the same control principle can be applied more broadly (e.g., context caching, tool/evidence invocation, selective summarization, or other budgeted allocation settings) without changing the downstream generator.

### CURVPRUNE: Curvature-Guided Budgeted Prompts.

Given a query/instruction  $q$  and a long context  $x$  that exceeds a token budget  $B$ , CURVPRUNE produces a pruned context  $\tilde{x}$  with  $|\tilde{x}| \leq B$  by scoring spans of  $x$  using aggregated curvature and retaining the highest-value spans (while preserving order). Intuitively, high-magnitude curvature marks locations where two-sided evidence either sharply focuses meaning (often worth retaining verbatim) or persistently fans out (often where context is underdetermined and thus important). We keep the main text lightweight and defer the span-scoring definition, sparse curvature estimation, and pseudocode to Appendix E.2 and Appendix E.4.

### CURVFLAG: Curvature-Guided Retrieval Routing.

Retrieval-augmented pipelines require (i) a *routing* decision—whether to retrieve and how much to retrieve—and (ii) a *targeting* strategy—which parts of the query/draft are responsible for underdetermination. CURVFLAG aggregates fan-out evidence into a scalar trigger that sets a retrieval budget and (optionally) falls back to full-context processing for saturated cases. The concrete routing map and the implementation details for chunking and query augmentation (e.g., curvature-aligned boundaries and anchor extraction) are engineering choices that we therefore place in Appendix E.3, along with pseudocode in Appendix E.4.

## 7. Experiments

We evaluate the *utility* of Texture as an inference-time control signal for long-context workloads. Parts I–II (existence certificates and the Texture operator) are evaluated and discussed in their respective sections; here we focus exclusively on whether curvature is actionable for budgeted context selection and retrieval routing.

All curvature quantities (boundary beliefs, bridges, and  $\kappa$ ) are computed using a frozen masked language model as a belief oracle (`distilroberta-base`), while downstream generation uses Meta-Llama-3-8B-Instruct without fine-tuning. We evaluate on five representative Long-Bench tasks spanning multi-hop QA, long-document QA, and long-context summarization (Bai et al., 2023): HotpotQA (Yang et al., 2018), 2WikiMultiHopQA (Ho et al., 2020), Qasper, GovReport, and QMSum (Zhong et al., 2021). Unless stated otherwise, tables report mean and standard deviation over examples; paired comparisons ad-

ditionally use bootstrap intervals over per-example deltas (Appendix E.5).

**Baselines.** For pruning/compression we compare against heuristic selection (random, recency, head+tail), query-aware relevance selection via BM25 (Robertson & Zaragoza, 2009), and learned prompt compression including Selective Context (Li et al., 2023) and LLMLingua (Jiang et al., 2023a). For routing/retrieval we compare against fixed- $k$  retrieval, FLARE (Jiang et al., 2023b), and Self-Route (Li et al., 2024).

### 7.1. Part III: Utility—Curvature-Guided Long-Context Control

We instantiate two curvature-controlled utilities. CURVPRUNE selects spans from an overlong context to satisfy a context budget  $B$  (context-only tokens, excluding the instruction/query), using curvature-derived span scores computed from longitudinal Texture. CURVFLAG routes between a retrieval-style pathway and a long-context pathway using a fan-out statistic (negative-curvature mass) to set retrieval budget and trigger retrieval. To isolate the effect of curvature, we emphasize paired “+Texture” variants that preserve a baseline’s primary signal and use Texture only as a secondary controller (e.g., BM25→BM25+Texture for budget allocation among BM25 candidates; FLARE→FLARE+Texture for the retrieval trigger).

We treat curvature as a secondary control signal that modulates baseline decisions without replacing them. For example, *BM25 + Texture* ranks spans by BM25 relevance, keeps top- $m$  as anchors, then allocates remaining budget via curvature-derived scores. Analogous constructions apply to routing (curvature mass modulates the retrieval trigger) and compression (curvature guides token-level allocation). Table 1 reports results at  $B=2048$ . BM25 is a strong baseline for multi-hop QA; Texture-augmented variants either use CURVPRUNE standalone or modulate an existing selector (e.g., BM25+Texture). Full budget sweeps are in Appendix E.5. Table 2 reports routing on multi-hop QA at a fixed cost target  $T$ , comparing curvature-based triggers against Self-Route and FLARE. Cost-quality frontiers and mechanism checks are in Appendix E.5.

**Analysis.** Pairwise comparisons (Table 7 in the Appendix) show that Texture provides consistent gains across both multi-hop QA benchmarks: routing yields +6–7 F1 on HotpotQA and +3.3 F1 on 2WikiMQA, while pruning gains +8.8 F1 on 2WikiMQA. The curvature signal is particularly effective for routing, where fan-out detection identifies when retrieval is beneficial versus when the full context should be preserved. For pruning, gains reflect Texture’s ability to prioritize bridge spans connecting disparate evidence—a

Table 1. Pruning on LongBench ( $B=2048$ ). F1 for QA; ROUGE-L for summarization. Mean  $\pm$  std.

Method	QA (F1)			Summ. (R-L)	
	Hotpot	2Wiki	Qasper	GovRep	QMSum
<i>Heuristic</i>					
Random	<b>28.4</b> $\pm$ 3.2	8.8 $\pm$ 1.9	6.3 $\pm$ 1.4	20.6 $\pm$ 2.1	14.6 $\pm$ 1.3
Recency	12.2 $\pm$ 2.5	6.6 $\pm$ 1.7	7.7 $\pm$ 1.6	19.1 $\pm$ 1.8	13.6 $\pm$ 1.1
Head+Tail	8.2 $\pm$ 2.1	10.3 $\pm$ 2.2	8.2 $\pm$ 1.5	20.4 $\pm$ 2.0	14.5 $\pm$ 1.2
<i>Query-Aware</i>					
BM25	27.3 $\pm$ 3.0	3.4 $\pm$ 1.2	9.5 $\pm$ 1.8	20.3 $\pm$ 1.9	<b>15.6</b> $\pm$ 1.2
<i>Compression</i>					
Sel. Ctx	20.1 $\pm$ 2.8	8.2 $\pm$ 1.8	7.4 $\pm$ 1.5	19.7 $\pm$ 1.9	14.6 $\pm$ 1.2
LLMLingua	18.8 $\pm$ 2.6	6.3 $\pm$ 1.6	5.9 $\pm$ 1.3	19.8 $\pm$ 1.8	14.7 $\pm$ 1.1
<i>+Texture</i>					
BM25+Tex	27.0 $\pm$ 3.0	12.2 $\pm$ 2.3	9.3 $\pm$ 1.7	20.5 $\pm$ 1.8	15.4 $\pm$ 1.2
<i>Ours</i>					
CurvPrune	27.8 $\pm$ 3.1	<b>13.1</b> $\pm$ 2.4	<b>10.2</b> $\pm$ 1.9	<b>21.0</b> $\pm$ 2.0	15.3 $\pm$ 1.2

Table 2. Routing on multi-hop QA. F1 and tokens at cost target  $T$ . +Tex. = Texture trigger.

Method	HotpotQA		2WikiMQA	
	F1	Toks	F1	Toks
<i>Adaptive</i>				
FLARE	21.4 $\pm$ 2.9	163	8.7 $\pm$ 1.8	173
Self-Route	18.6 $\pm$ 2.7	9271	7.2 $\pm$ 1.6	5712
<i>+Texture</i>				
FLARE+Tex	28.3 $\pm$ 3.2	155	12.0 $\pm$ 2.1	44
SelfRt+Tex	24.8 $\pm$ 3.0	301	10.5 $\pm$ 1.9	5680
<i>Ours</i>				
CurvFlag	<b>29.1</b> $\pm$ 3.3	<b>148</b>	<b>12.8</b> $\pm$ 2.2	<b>41</b>

structure common in multi-hop reasoning. These results confirm that curvature captures task-relevant structure beyond lexical relevance (BM25) or learned compression alone.

## 8. Conclusion

We presented a unified framework for *text curvature* built around three goals: **existence**, **definition**, and **utility**. First, we provided definition-robust non-flatness certificates—holonomy and CEI—and empirically falsified both flatness nulls (Section 4). Second, we introduced Texture: a computable curvature operator that reconciles left- and right-context beliefs via a Schrödinger bridge midpoint (Section 5). Third, we showed how curvature serves as an inference-time control primitive for compression and retrieval routing (Sections 6–7). Looking ahead, key directions include connecting this discrete curvature to continuous Ricci-type quantities via heat-kernel limits, learning task-aware neutral kernels, and applying curvature fields to controllable generation and uncertainty estimation.

## Impact Statement

**Potential benefits.** This work proposes a text-native curvature measurement and demonstrates its use as an inference-time control signal. If validated at scale, curvature-guided compression and retrieval routing could reduce compute and latency in LLM systems, improving accessibility and lowering environmental and monetary costs. Curvature-based diagnostics may also improve interpretability by highlighting structurally pivotal regions in prompts and documents.

**Potential risks and misuse.** Curvature-guided selection can amplify biases present in the belief extractor or in the underlying corpora: if a model systematically assigns fan-out/focus in biased ways, retrieval and compression decisions may preferentially preserve or discard certain viewpoints. RAG systems may inadvertently retrieve harmful or misleading content if retrieval is triggered in sensitive fan-out regions. We mitigate these risks by (i) reporting bias-sensitive analyses when feasible, (ii) recommending conservative thresholds and human oversight for high-stakes domains, and (iii) isolating failure modes where curvature signals become unreliable.

**Data and privacy.** Our experiments use public datasets and do not require collecting new personal data. For any dataset with human behavioral measurements (reading time/eye tracking), we follow dataset licenses and ethical usage norms and report only aggregate analyses.

## References

Ambrosio, L., Gigli, N., and Savaré, G. *Gradient flows: in metric spaces and in the space of probability measures*. Springer, 2005.

Angeli, G., Premkumar, M. J. J., and Manning, C. D. Leveraging linguistic structure for open domain information extraction. In *Proceedings of the 53rd Annual Meeting of the Association for Computational Linguistics and the 7th International Joint Conference on Natural Language Processing (Volume 1: Long Papers)*, pp. 344–354, 2015.

Bai, Y., Lv, X., Zhang, J., Lyu, H., Tang, J., Huang, Z., Du, Z., Liu, X., Zeng, A., Hou, L., Dong, Y., Tang, J., and Li, J. Longbench: A bilingual, multitask benchmark for long context understanding. *ArXiv*, abs/2308.14508, 2023. URL <https://api.semanticscholar.org/CorpusID:261245264>.

Banarescu, L., Bonial, C., Cai, S., Georgescu, M., Griffitt, K., Hermjakob, U., Knight, K., Koehn, P., Palmer, M., and Schneider, N. Abstract meaning representation for sembanking. In *Proceedings of the 7th linguistic annotation workshop and interoperability with discourse*, pp. 178–186, 2013.

Chen, W., Han, X., Lin, Y., He, K., Xie, R., Zhou, J., Liu, Z., and Sun, M. Hyperbolic pre-trained language model. *IEEE/ACM Transactions on Audio, Speech, and Language Processing*, 32:3101–3112, 2024.

Cuturi, M. Sinkhorn distances: Lightspeed computation of optimal transport. In *Neural Information Processing Systems*, 2013. URL <https://api.semanticscholar.org/CorpusID:15966283>.

Devlin, J., Chang, M.-W., Lee, K., and Toutanova, K. Bert: Pre-training of deep bidirectional transformers for language understanding. In *North American Chapter of the Association for Computational Linguistics*, 2019. URL <https://api.semanticscholar.org/CorpusID:52967399>.

Etzioni, O., Banko, M., Soderland, S., and Weld, D. S. Open information extraction from the web. *Communications of the ACM*, 51(12):68–74, 2008.

Forman, R. Bochner’s method for cell complexes and combinatorial ricci curvature. *Discrete & Computational Geometry*, 29:323–374, 2003. URL <https://api.semanticscholar.org/CorpusID:9584267>.

Ganea, O., Bécigneul, G., and Hofmann, T. Hyperbolic neural networks. *Advances in neural information processing systems*, 31, 2018.

Gokaslan, A. and Cohen, V. Openwebtext corpus. <http://Skylion007.github.io/OpenWebTextCorpus>, 2019.

Grover, K., Yu, H., Song, X., Zhu, Q., Xie, H., Ioannidis, V. N., and Faloutsos, C. Spectro-riemannian graph neural networks. *arXiv preprint arXiv:2502.00401*, 2025.

Gu, A., Sala, F., Gunel, B., and Ré, C. Learning mixed-curvature representations in product spaces. In *International conference on learning representations*, 2018.

He, N., Liu, J., Zhang, B., Bui, N., Maatouk, A., Yang, M., King, I., Weber, M., and Ying, R. Position: Beyond euclidean–foundation models should embrace non-euclidean geometries. *arXiv preprint arXiv:2504.08896*, 2025.

Hinton, G. E. Products of experts. 1999. URL <https://api.semanticscholar.org/CorpusID:15059668>.

Ho, X., Duong Nguyen, A.-K., Sugawara, S., and Aizawa, A. Constructing a multi-hop QA dataset for comprehensive evaluation of reasoning steps. In *Proceedings of the 28th International Conference on Computational Linguistics*, pp. 6609–6625, Barcelona, Spain (Online),

December 2020. International Committee on Computational Linguistics. URL <https://www.aclweb.org/anthology/2020.coling-main.580>.

Jiang, H., Wu, Q., Lin, C.-Y., Yang, Y., and Qiu, L. Llmlingua: Compressing prompts for accelerated inference of large language models. In *Conference on Empirical Methods in Natural Language Processing*, 2023a. URL <https://api.semanticscholar.org/CorpusID:263830701>.

Jiang, Z., Xu, F. F., Gao, L., Sun, Z., Liu, Q., Dwivedi-Yu, J., Yang, Y., Callan, J., and Neubig, G. Active retrieval augmented generation, 2023b. URL <https://arxiv.org/abs/2305.06983>.

L'eonard, C. A survey of the schrödinger problem and some of its connections with optimal transport. *arXiv: Probability*, 2013. URL <https://api.semanticscholar.org/CorpusID:14387241>.

Lewis, P., Perez, E., Piktus, A., Petroni, F., Karpukhin, V., Goyal, N., Kuttler, H., Lewis, M., tau Yih, W., Rocktäschel, T., Riedel, S., and Kiela, D. Retrieval-augmented generation for knowledge-intensive nlp tasks. *ArXiv*, abs/2005.11401, 2020. URL <https://api.semanticscholar.org/CorpusID:218869575>.

Li, Y., Dong, B., Lin, C., and Guerin, F. Compressing context to enhance inference efficiency of large language models, 2023.

Li, Z., Li, C., Zhang, M., Mei, Q., and Bender-sky, M. Retrieval augmented generation or long-context llms? a comprehensive study and hybrid approach. *ArXiv*, abs/2407.16833, 2024. URL <https://api.semanticscholar.org/CorpusID:271404721>.

Liu, Y., Ott, M., Goyal, N., Du, J., Joshi, M., Chen, D., Levy, O., Lewis, M., Zettlemoyer, L., and Stoyanov, V. Roberta: A robustly optimized bert pretraining approach. *ArXiv*, abs/1907.11692, 2019. URL <https://api.semanticscholar.org/CorpusID:198953378>.

Merity, S., Xiong, C., Bradbury, J., and Socher, R. Pointer sentinel mixture models. *ArXiv*, abs/1609.07843, 2016. URL <https://api.semanticscholar.org/CorpusID:16299141>.

Ni, L. Holonomy and the ricci curvature of complex hermitian manifolds. *The Journal of Geometric Analysis*, 35, 2024. URL <https://api.semanticscholar.org/CorpusID:273228264>.

Nickel, M. and Kiela, D. Poincaré embeddings for learning hierarchical representations. *Advances in neural information processing systems*, 30, 2017.

Ollivier, Y. Ricci curvature of markov chains on metric spaces. *Journal of Functional Analysis*, 256:810–864, 2007. URL <https://api.semanticscholar.org/CorpusID:14316364>.

Robertson, S. E. and Zaragoza, H. The probabilistic relevance framework: Bm25 and beyond. *Found. Trends Inf. Retr.*, 3:333–389, 2009. URL <https://api.semanticscholar.org/CorpusID:207178704>.

Samson, P.-M. Entropic curvature on graphs along schrödinger bridges at zero temperature. *Probability Theory and Related Fields*, 184(3–4):859–937, October 2022. ISSN 1432-2064. doi: 10.1007/s00440-022-01167-4. URL <http://dx.doi.org/10.1007/s00440-022-01167-4>.

Sanh, V., Debut, L., Chaumond, J., and Wolf, T. Distilbert, a distilled version of bert: smaller, faster, cheaper and lighter. *ArXiv*, abs/1910.01108, 2019.

Sia, J., Jonckheere, E., and Bogdan, P. Ollivier-ricci curvature-based method to community detection in complex networks. *Scientific reports*, 9(1):9800, 2019.

Sreejith, R. P., Mohanraj, K. G., Jost, J., Jost, J., Saucan, E., Saucan, E., and Samal, A. Forman curvature for complex networks. *Journal of Statistical Mechanics: Theory and Experiment*, 2016, 2016. URL <https://api.semanticscholar.org/CorpusID:6529015>.

Yang, Z., Qi, P., Zhang, S., Bengio, Y., Cohen, W. W., Salakhutdinov, R., and Manning, C. D. Hotpotqa: A dataset for diverse, explainable multi-hop question answering. In *Conference on Empirical Methods in Natural Language Processing*, 2018. URL <https://api.semanticscholar.org/CorpusID:52822214>.

Zhong, M., Yin, D., Yu, T., Zaidi, A., Mutuma, M., Jha, R., Awadallah, A. H., Celikyilmaz, A., Liu, Y., Qiu, X., and Radev, D. Qmsum: A new benchmark for query-based multi-domain meeting summarization, 2021. URL <https://arxiv.org/abs/2104.05938>.

## Appendix

### Contents of the Appendix

A. Notation Reference .....	12
B. Additional Theory for Existence Certificates (Part I) .....	13
B.1. Holonomy and Discrete Integrability of Log-Odds .....	13
B.2. Evidence Additivity and Product-of-Experts (CEI) .....	15
B.3. Empirical Setup Details .....	17
B.4. Additional Empirical Diagnostics .....	17
C. Additional Theory for Texture Curvature (Part II) .....	17
C.1. Neutral Kernel: Reversibility from a Symmetric Cost .....	18
C.2. Two-Step Schrödinger Bridge: Reduction, Scaling Form, and Midpoint Computation .....	19
C.3. Bridge Energy: Endpoint Identity, Dual Form, and Symmetry .....	21
C.4. Deriving the Curvature Readout and the Factor 8 .....	22
C.5. Stability and Truncation Consistency .....	22
C.6. Algorithmic Summary .....	23
C.7. Transversal Texture: Curvature on Relational Graphs .....	24
D. Utility Controllers (Part III) .....	26
D.1. Sparse Curvature Estimation for Control .....	26
D.2. CURVPRUNE: Span Scoring and Guard Bands .....	27
D.3. CURVFLAG: Routing, Chunking, and Anchors .....	27
D.4. Algorithms and Complexity .....	27
D.5. Additional Experimental Results .....	28
E. Experimental Details .....	12
E.1. Compute Environment and Reproducibility .....	12
E.2. Token Accounting and Budget Matching .....	13
E.3. Statistical Reporting .....	13

## A. Notation Reference

Table 3 summarizes notation used throughout; detailed definitions appear in the indicated sections.

Table 3. Summary of notation.

Symbol	Description	Ref.
<i>Text, Slots, and Beliefs</i>		
$x_{1:n}, x_{<i}, x_{>i}$	Token sequence; prefix; suffix	§3
$x_{<i}^L, x_{>i}^R$	Truncated contexts of radii $L, R$	§3
$(x_{<i}, \square, x_{>i})$	Contextual slot at position $i$	§3
$\mathcal{S}_i, \mathcal{C}_i, \text{tail}$	State space; candidate set; tail bucket	§3
$\Delta(\mathcal{S}), \Delta^\circ(\mathcal{S})$	Simplex; interior (full support)	§3
$\mu_i^L, \mu_i^R$	Left/right boundary beliefs	§5
$\mu_i(L, R)$	Two-sided posterior at radii $(L, R)$	§4
$\mathcal{B}_{\leftrightarrow}$	Two-sided belief extractor	§3
<i>Existence Certificates (Part I)</i>		
$\text{KL}(\mu \parallel \nu)$	Kullback–Leibler divergence	§3
$u_{i,s}(L, R)$	Log-odds: $\log[\mu_i(L, R)(s)/\mu_i(L, R)(s_{\text{ref}})]$	§4
$\Omega_{i,s}(L, R), h_i$	Unit-square holonomy; aggregated magnitude	§4
$\mu_i^{\leftarrow}, \mu_i^{\rightarrow}, \mu_i^{(0)}$	Left-only, right-only, base beliefs	§4
$\mu_i^{\text{PoE}}, \text{CEI}_i$	Product-of-Experts; contextual evidence interaction	§4
<i>Neutral Kernel and Dynamics (Part II)</i>		
$c_i(s, s'), \varepsilon$	Symmetric ground cost; temperature	§5
$G_i, K_i, \pi_i$	Gibbs affinity; Markov kernel; stationary dist.	§5
$R_i(s_0, s_1, s_2)$	Reference path: $\pi_i(s_0)K_i(s_0, s_1)K_i(s_1, s_2)$	§5
<i>Schrödinger Bridge and Curvature (Part II)</i>		
$P_i^*$	Optimal bridge path measure	§5
$\mu_i^{\text{mid}}$	Bridge midpoint: $(P_i^*)_1$	§5
$(a, b), \gamma^*, R_{02}$	Scaling vectors; endpoint coupling; reference	App. D.2
$\Phi_i(\rho)$	Free energy: $\text{KL}(\rho \parallel \pi_i)$	§5
$\Delta_i^\Phi$	Midpoint gap: $\frac{1}{2}[\Phi(\mu_i^L) + \Phi(\mu_i^R)] - \Phi(\mu_i^{\text{mid}})$	§5
$D_i^2, \epsilon_0$	Bridge energy $\text{KL}(P_i^* \parallel R_i)$ ; numerical guard	§5
$\kappa_i$	<b>Texture curvature:</b> $8\Delta_i^\Phi/(D_i^2 + \epsilon_0)$	§5
<i>Utility Controllers (Part III)</i>		
$B, k$	Token budget; retrieval budget	§6
$s(I), (w_-, w_+)$	Span score; fan-out/focus weights	App. E
$M_-(z)$	Fan-out mass: $\sum_i [-\kappa_i]_+$	App. E

**Conventions.** Subscript  $i$  denotes slot index. We write  $\propto$  for equality up to normalization and  $[x]_+ := \max(x, 0)$  for the positive part. When clear from context, slot subscripts may be suppressed.

## B. Additional Experimental Details

This appendix provides full experimental protocol details and additional context for reproducibility.

### B.1. Compute Environment and Reproducibility

All runs are executed with fixed random seeds and fully specified configuration files. We log: (a) the repository commit hash, (b) dataset versions/\_hashes, (c) model identifiers and revisions, (d) prompt templates, (e) budgets and hyperparameters, and (f) decoding settings. Geometric quantities are computed using a frozen MLM belief oracle (`distilroberta-base`). Downstream generation uses `Meta-Llama-3-8B-Instruct`. Curvature and belief computations are cached per (query, context, configuration, model revision) key and reused across budget sweeps.

## B.2. Token Accounting and Budget Matching

For pruning we enforce a context-token budget  $B$  that counts only the selected evidence/context tokens; instruction boilerplate is held fixed across methods and excluded from  $B$ . Token counts are computed with the downstream generator tokenizer to reflect actual inference cost. We enforce budget fill by requiring budgeted methods to use at least  $0.98B$  tokens on average. For routing, total-token cost includes prompt, selected/retrieved context, and generated output up to the maximum new-token cap. We select the best hyperparameter setting for each routing method subject to  $\mathbb{E}[\text{tokens}] \leq T$ ; we use  $T = 2048$  in the main paper.

## B.3. Statistical Reporting

We compute 95% bootstrap confidence intervals with 1000 resamples. For paired comparisons (baseline vs. baseline+Texture), we compute per-example deltas and bootstrap the mean delta to obtain paired intervals.

## B.4. Part I (Existence) Experimental Details

We sample slots from WikiText-2 (raw) and OpenWebText-10k following the Part I protocol for slot selection and context windows. Beliefs  $\mu^L, \mu^R$  are computed with the frozen MLM belief oracle and converted into log-odds updates as described in Section 4. We evaluate two control conditions: (i) swap controls that exchange left/right contexts across examples and (ii) shuffle controls that permute words within local windows, preserving marginal statistics but breaking coherent composition. Natural text exhibits systematic deviations from flatness nulls, with elevated holonomy magnitudes and non-trivial CEI values, while both controls collapse toward flat behavior.

## B.5. Part II (Definition) Stability

The Texture curvature field is stable across modeling choices. We verified stability with respect to: (i) support size  $k \in \{10, 20, 50, 100\}$ , showing high rank correlation across choices; (ii) kernel temperature  $\varepsilon$ , with consistent sign patterns across a sweep; and (iii) context radii  $(L, R)$  phase diagrams confirming that curvature emerges specifically from two-sided coherent composition.

## B.6. Part III (Utility) Extended Details

We follow LongBench’s standardized format and evaluation scripts. Prompt templates, decoding parameters, and answer post-processing rules are reported alongside the released code. Query-aware span selection uses BM25; learned compression baselines include Selective Context and LLMLingua; routing baselines include FLARE and Self-Route.

## C. Additional Theory for Section 4

This appendix provides the full statements and proofs of the two *definition-independent* certificates used in Section 4. Both results are phrased as falsifiable *flatness nulls* on the two-sided posterior field  $(L, R) \mapsto \mu_i(L, R)$ . Throughout, we assume full support  $(\mu_i(L, R) \in \Delta^\circ(\mathcal{S}_i))$ ; empirically this is ensured by a tail bucket and/or an  $\varepsilon$ -smoothing.

### C.1. Certificate I: Holonomy and Discrete Integrability of Log-Odds

**Theorem C.1** (Holonomy characterization of log-odds separability). *Curvature certificate (falsifiable flatness null). Define the unit-square holonomy  $\Omega_{i,s}(L, R)$  from the two-sided belief field. If there exist a state  $s \in \mathcal{S}_i$  and an adjacent grid cell  $(L, R)$  such that  $\Omega_{i,s}(L, R) \neq 0$ , then the flatness null fails: the log-odds field is not additively separable in  $(L, R)$ , hence the two-sided inference geometry exhibits genuine left-right interaction.*

Setup. Fix a slot  $i$  and a finite candidate/state set  $\mathcal{S}_i$ . Let  $L_{\max}, R_{\max} \in \mathbb{N}$  and define the discrete grid domain

$$\mathcal{D} := \{0, 1, \dots, L_{\max}\} \times \{0, 1, \dots, R_{\max}\}.$$

(Only adjacency on the grid matters; if one uses nonuniform radii in practice, re-index them by their grid positions.) Assume a strictly positive belief field  $\mu_i(L, R) \in \Delta^\circ(\mathcal{S}_i)$  for each  $(L, R) \in \mathcal{D}$ .

Fix an arbitrary reference state  $s_{\text{ref}} \in \mathcal{S}_i$  and define the log-odds field

$$u_{i,s}(L, R) := \log \frac{\mu_i(L, R)(s)}{\mu_i(L, R)(s_{\text{ref}})} \quad (s \in \mathcal{S}_i, (L, R) \in \mathcal{D}). \quad (14)$$

Define the unit-square holonomy for  $0 \leq L < L_{\max}$  and  $0 \leq R < R_{\max}$  by

$$\Omega_{i,s}(L, R) := u_{i,s}(L+1, R+1) - u_{i,s}(L+1, R) - u_{i,s}(L, R+1) + u_{i,s}(L, R). \quad (15)$$

Claim (equivalence). The following are equivalent:

$$\Omega_{i,s}(L, R) = 0 \text{ for all } s \in \mathcal{S}_i \text{ and all unit squares } (L, R), \quad (16)$$

and for every  $s \in \mathcal{S}_i$  there exist functions  $\alpha_{i,s} : \{0, \dots, L_{\max}\} \rightarrow \mathbb{R}$  and  $\beta_{i,s} : \{0, \dots, R_{\max}\} \rightarrow \mathbb{R}$  with  $\alpha_{i,s}(0) = \beta_{i,s}(0) = 0$  such that

$$u_{i,s}(L, R) = u_{i,s}(0, 0) + \alpha_{i,s}(L) + \beta_{i,s}(R) \quad \text{for all } (L, R) \in \mathcal{D}. \quad (17)$$

Discrete Stokes / telescoping identity. For any rectangle  $0 \leq L_1 < L_2 \leq L_{\max}$  and  $0 \leq R_1 < R_2 \leq R_{\max}$ , define the rectangle holonomy

$$\mathcal{H}_{i,s}(L_1, L_2, R_1, R_2) := u_{i,s}(L_2, R_2) - u_{i,s}(L_2, R_1) - u_{i,s}(L_1, R_2) + u_{i,s}(L_1, R_1). \quad (18)$$

Then  $\mathcal{H}_{i,s}$  decomposes into the sum of unit-square holonomies:

$$\mathcal{H}_{i,s}(L_1, L_2, R_1, R_2) = \sum_{\ell=L_1}^{L_2-1} \sum_{r=R_1}^{R_2-1} \Omega_{i,s}(\ell, r). \quad (19)$$

*Proof.* We first prove the telescoping identity (19), then prove the equivalence between the flatness null (16) and the additive decomposition (17).

**Step 1: telescoping over a rectangle (proof of (19)).** Fix  $s \in \mathcal{S}_i$  and a rectangle  $(L_1, L_2, R_1, R_2)$ . Sum (15) over  $r = R_1, \dots, R_2 - 1$  for a fixed  $\ell$ :

$$\begin{aligned} \sum_{r=R_1}^{R_2-1} \Omega_{i,s}(\ell, r) &= \sum_{r=R_1}^{R_2-1} (u_{i,s}(\ell+1, r+1) - u_{i,s}(\ell+1, r)) - \sum_{r=R_1}^{R_2-1} (u_{i,s}(\ell, r+1) - u_{i,s}(\ell, r)) \\ &= (u_{i,s}(\ell+1, R_2) - u_{i,s}(\ell+1, R_1)) - (u_{i,s}(\ell, R_2) - u_{i,s}(\ell, R_1)), \end{aligned}$$

because each sum telescopes. Now sum this identity over  $\ell = L_1, \dots, L_2 - 1$ ; telescoping again yields

$$\sum_{\ell=L_1}^{L_2-1} \sum_{r=R_1}^{R_2-1} \Omega_{i,s}(\ell, r) = u_{i,s}(L_2, R_2) - u_{i,s}(L_2, R_1) - u_{i,s}(L_1, R_2) + u_{i,s}(L_1, R_1) = \mathcal{H}_{i,s}(L_1, L_2, R_1, R_2),$$

which is (19).

**Step 2: additive decomposition  $\Rightarrow$  zero holonomy.** Assume (17). Substituting it into (15) shows all terms cancel:

$$\begin{aligned} \Omega_{i,s}(L, R) &= (u_{i,s}(0, 0) + \alpha_{i,s}(L+1) + \beta_{i,s}(R+1)) - (u_{i,s}(0, 0) + \alpha_{i,s}(L+1) + \beta_{i,s}(R)) \\ &\quad - (u_{i,s}(0, 0) + \alpha_{i,s}(L) + \beta_{i,s}(R+1)) + (u_{i,s}(0, 0) + \alpha_{i,s}(L) + \beta_{i,s}(R)) = 0. \end{aligned}$$

Thus (16) holds.

**Step 3: zero holonomy  $\Rightarrow$  additive decomposition.** Assume (16). By Step 1,  $\Omega \equiv 0$  implies  $\mathcal{H} \equiv 0$  on every rectangle. In particular, for the rectangle with corners  $(0, 0), (L, 0), (0, R), (L, R)$  we obtain

$$0 = \mathcal{H}_{i,s}(0, L, 0, R) = u_{i,s}(L, R) - u_{i,s}(L, 0) - u_{i,s}(0, R) + u_{i,s}(0, 0),$$

hence

$$u_{i,s}(L, R) = u_{i,s}(L, 0) + u_{i,s}(0, R) - u_{i,s}(0, 0). \quad (20)$$

Define

$$\alpha_{i,s}(L) := u_{i,s}(L, 0) - u_{i,s}(0, 0), \quad \beta_{i,s}(R) := u_{i,s}(0, R) - u_{i,s}(0, 0), \quad (21)$$

so  $\alpha_{i,s}(0) = \beta_{i,s}(0) = 0$ . Substituting (21) into (20) yields exactly (17).

**Step 4: certificate interpretation.** Steps 2–3 show that (16) is equivalent to additive separability (17). Therefore if any unit-square holonomy is nonzero, the additive decomposition cannot hold, which is precisely the stated curvature certificate.  $\square$

**Remark (reference-state / gauge invariance).** Changing the reference state in (14) applies a gauge transformation to the log-odds coordinates: if  $u'_{i,s}(L, R) = \log \frac{\mu_i(L, R)(s)}{\mu_i(L, R)(s'_{\text{ref}})}$ , then  $u'_{i,s}(L, R) = u_{i,s}(L, R) - u_{i,s'_{\text{ref}}}(L, R)$ . Taking the mixed difference (15) gives  $\Omega'_{i,s}(L, R) = \Omega_{i,s}(L, R) - \Omega_{i,s'_{\text{ref}}}(L, R)$ . Consequently, the flatness null “ $\Omega_{i,s}(L, R) = 0$  for all  $s$  and all unit squares” is invariant to the choice of reference. Moreover, the curvature certificate is also invariant: if some  $\Omega_{i,s}$  is nonzero under one reference, then not all  $\Omega'_{i,s}$  can vanish under another reference because  $\Omega'_{i,s'_{\text{ref}}} \equiv 0$  by construction.

## C.2. Certificate II: Evidence Additivity and Product-of-Experts (CEI)

**Theorem C.2** (Product-of-Experts characterization of evidence additivity). Curvature certificate (falsifiable flatness null). Fix  $(L, R)$ . Define the PoE reconstruction  $\mu_i^{\text{PoE}}(L, R)$  from the boundary beliefs  $\mu_i(L, 0)$  and  $\mu_i(0, R)$  and the base belief  $\mu_i(0, 0)$ . If  $\mu_i(L, R) \neq \mu_i^{\text{PoE}}(L, R)$  (equivalently  $\text{CEI}_i(L, R) > 0$ ), then the additive-evidence flatness null fails: left and right context interact beyond additive log Bayes factors.

Setup. Fix a slot  $i$  and a finite candidate/state set  $\mathcal{S}_i$ . Assume a strictly positive two-sided belief field  $\mu_i(L, R) \in \Delta^\circ(\mathcal{S}_i)$ . For a fixed pair of radii  $(L, R)$  define the one-sided boundary beliefs

$$\mu_i^{\leftarrow}(L) := \mu_i(L, 0), \quad \mu_i^{\rightarrow}(R) := \mu_i(0, R), \quad \mu_i^{(0)} := \mu_i(0, 0).$$

Define the (normalized) product-of-experts reconstruction by

$$\mu_i^{\text{PoE}}(L, R)(s) := \frac{1}{Z_i(L, R)} \frac{\mu_i^{\leftarrow}(L)(s) \mu_i^{\rightarrow}(R)(s)}{\mu_i^{(0)}(s)}, \quad Z_i(L, R) := \sum_{t \in \mathcal{S}_i} \frac{\mu_i^{\leftarrow}(L)(t) \mu_i^{\rightarrow}(R)(t)}{\mu_i^{(0)}(t)}. \quad (22)$$

Define the Contextual Evidence Interaction statistic

$$\text{CEI}_i(L, R) := \text{KL}\left(\mu_i(L, R) \parallel \mu_i^{\text{PoE}}(L, R)\right) \geq 0. \quad (23)$$

Claim 1 (PoE-flatness null  $\iff$  additive Bayes factors). The following are equivalent:

$$\begin{aligned} \mu_i(L, R) &= \mu_i^{\text{PoE}}(L, R) \\ \iff \exists c(L, R) &\in \mathbb{R} \text{ s.t.} \\ \log \mu_i(L, R)(s) &= \log \mu_i^{\leftarrow}(L)(s) + \log \mu_i^{\rightarrow}(R)(s) - \log \mu_i^{(0)}(s) + c(L, R) \end{aligned}$$

for all  $s \in \mathcal{S}_i$ . Consequently,

$$\text{CEI}_i(L, R) = 0 \iff \mu_i(L, R) = \mu_i^{\text{PoE}}(L, R). \quad (24)$$

Claim 2 (variational characterization). Define, for  $q \in \Delta(\mathcal{S}_i)$ ,

$$\mathcal{J}_{i,L,R}(q) := \text{KL}(q \parallel \mu_i^{\leftarrow}) + \text{KL}(q \parallel \mu_i^{\rightarrow}) - \text{KL}(q \parallel \mu_i^{(0)}). \quad (25)$$

Then  $\mathcal{J}_{i,L,R}$  admits the exact identity

$$\mathcal{J}_{i,L,R}(q) = \text{KL}\left(q \parallel \mu_i^{\text{PoE}}(L, R)\right) - \log Z_i(L, R), \quad (26)$$

so  $\mu_i^{\text{PoE}}(L, R)$  is the unique minimizer of  $\mathcal{J}_{i,L,R}$  and

$$\text{CEI}_i(L, R) = \mathcal{J}_{i,L,R}(\mu_i(L, R)) - \min_{q \in \Delta(\mathcal{S}_i)} \mathcal{J}_{i,L,R}(q). \quad (27)$$

**Claim 3 (generative sufficiency).** Let  $Z \in \mathcal{S}_i$  be the slot value and let  $X^L, X^R$  denote the left/right context observations at radii  $(L, R)$ . If the beliefs correspond to exact posteriors  $\mu_i(L, R)(\cdot) = \mathbb{P}(Z = \cdot | X^L, X^R)$ ,  $\mu_i^{\leftarrow}(\cdot) = \mathbb{P}(Z = \cdot | X^{\leftarrow})$ ,  $\mu_i^{\rightarrow}(\cdot) = \mathbb{P}(Z = \cdot | X^{\rightarrow})$ ,  $\mu_i^{(0)}(\cdot) = \mathbb{P}(Z = \cdot)$ , and if  $X^{\leftarrow} \perp X^{\rightarrow} | Z$ , then  $\mu_i(L, R) = \mu_i^{\text{PoE}}(L, R)$  for every realization with positive probability.

*Proof.* **Step 1: Claim 1 (PoE  $\Leftrightarrow$  additive Bayes factors).** Assume there exists  $c(L, R)$  such that

$$\log \mu_i(L, R)(s) = \log \mu_i^{\leftarrow}(L)(s) + \log \mu_i^{\rightarrow}(R)(s) - \log \mu_i^{(0)}(s) + c(L, R) \quad \text{for all } s.$$

Exponentiating gives

$$\mu_i(L, R)(s) = e^{c(L, R)} \frac{\mu_i^{\leftarrow}(L)(s) \mu_i^{\rightarrow}(R)(s)}{\mu_i^{(0)}(s)}.$$

Summing both sides over  $s$  and using  $\sum_s \mu_i(L, R)(s) = 1$  yields  $e^{c(L, R)} = 1/Z_i(L, R)$ , hence  $\mu_i(L, R) = \mu_i^{\text{PoE}}(L, R)$ .

Conversely, if  $\mu_i(L, R) = \mu_i^{\text{PoE}}(L, R)$ , then by (22)

$$\mu_i(L, R)(s) = \frac{1}{Z_i(L, R)} \frac{\mu_i^{\leftarrow}(L)(s) \mu_i^{\rightarrow}(R)(s)}{\mu_i^{(0)}(s)},$$

and taking logs gives the additive identity with  $c(L, R) = -\log Z_i(L, R)$ . This proves Claim 1 and the zero-iff statement (24) follows from the basic property  $\text{KL}(P\|Q) = 0 \Leftrightarrow P = Q$ .

**Step 2: Claim 2 (variational identity).** Write  $\mu^{\leftarrow} := \mu_i^{\leftarrow}(L)$ ,  $\mu^{\rightarrow} := \mu_i^{\rightarrow}(R)$ ,  $\mu^{(0)} := \mu_i^{(0)}$  and abbreviate  $\mu^{\text{PoE}} := \mu_i^{\text{PoE}}(L, R)$ ,  $Z := Z_i(L, R)$ . Expand (25) using  $\text{KL}(q\|p) = \sum_s q(s) \log \frac{q(s)}{p(s)}$ :

$$\begin{aligned} \mathcal{J}_{i,L,R}(q) &= \sum_s q(s) \log \frac{q(s)}{\mu^{\leftarrow}(s)} + \sum_s q(s) \log \frac{q(s)}{\mu^{\rightarrow}(s)} - \sum_s q(s) \log \frac{q(s)}{\mu^{(0)}(s)} \\ &= \sum_s q(s) \log q(s) - \sum_s q(s) (\log \mu^{\leftarrow}(s) + \log \mu^{\rightarrow}(s) - \log \mu^{(0)}(s)). \end{aligned}$$

Define the unnormalized PoE density  $\tilde{\mu}^{\text{PoE}}(s) := \mu^{\leftarrow}(s) \mu^{\rightarrow}(s) / \mu^{(0)}(s)$  so that  $\mu^{\text{PoE}}(s) = \tilde{\mu}^{\text{PoE}}(s) / Z$  and hence  $\log \mu^{\text{PoE}}(s) = \log \tilde{\mu}^{\text{PoE}}(s) - \log Z$ . Then

$$\begin{aligned} \text{KL}(q\|\mu^{\text{PoE}}) &= \sum_s q(s) \log \frac{q(s)}{\mu^{\text{PoE}}(s)} = \sum_s q(s) \log q(s) - \sum_s q(s) \log \mu^{\text{PoE}}(s) \\ &= \sum_s q(s) \log q(s) - \sum_s q(s) \log \tilde{\mu}^{\text{PoE}}(s) + \log Z = \mathcal{J}_{i,L,R}(q) + \log Z, \end{aligned}$$

which rearranges to (26).

Because  $\mu^{\text{PoE}}$  has full support,  $\text{KL}(q\|\mu^{\text{PoE}})$  is strictly convex in  $q$  on the simplex. By (26),  $\mathcal{J}_{i,L,R}$  differs only by an additive constant, so it is strictly convex as well and has a unique minimizer. The unique minimizer is achieved when  $\text{KL}(q\|\mu^{\text{PoE}}) = 0$ , i.e.,  $q = \mu^{\text{PoE}}$ . Finally, plugging  $q = \mu_i(L, R)$  and  $q^* = \mu^{\text{PoE}}$  into (26) yields (27).

**Step 3: Claim 3 (conditional independence sufficiency).** Assume  $X^L \perp X^R | Z$  and fix any realization  $(x^L, x^R)$  with positive probability. Bayes' rule gives

$$\mathbb{P}(Z = z | x^L, x^R) \propto \mathbb{P}(x^L, x^R | Z = z) \mathbb{P}(Z = z) = \mathbb{P}(x^L | Z = z) \mathbb{P}(x^R | Z = z) \mathbb{P}(Z = z),$$

where the equality uses conditional independence. Rewrite each likelihood term via Bayes:

$$\mathbb{P}(x^L | Z = z) = \frac{\mathbb{P}(Z = z | x^L) \mathbb{P}(x^L)}{\mathbb{P}(Z = z)}, \quad \mathbb{P}(x^R | Z = z) = \frac{\mathbb{P}(Z = z | x^R) \mathbb{P}(x^R)}{\mathbb{P}(Z = z)}.$$

Table 4. **Certificate I (Holonomy): summary statistics.** Medians over 1000 slots per dataset.  $\Delta = \text{median}(\text{Real}) - \text{median}(\text{Control})$  with 95% bootstrap CIs.

Dataset	Median $h_i$			$\Delta$ [95% CI]	
	Real	Swap	Shuffle	Real–Swap	Real–Shuffle
WikiText-2	0.596	0.305	0.373	0.291 [0.27, 0.31]	0.223 [0.20, 0.25]
OpenWebText	0.586	0.326	0.391	0.260 [0.24, 0.29]	0.195 [0.18, 0.22]

Substituting and absorbing factors independent of  $z$  into the proportionality constant yields

$$\mathbb{P}(Z = z \mid x^L, x^R) \propto \frac{\mathbb{P}(Z = z \mid x^L) \mathbb{P}(Z = z \mid x^R)}{\mathbb{P}(Z = z)}.$$

Renormalizing over  $z \in \mathcal{S}_i$  gives exactly the PoE form (22), hence  $\mu_i(L, R) = \mu_i^{\text{PoE}}(L, R)$  and  $\text{CEI}_i(L, R) = 0$ .  $\square$

**Remark (information-theoretic interpretation).** Claim 3 identifies a concrete *generative* flatness null. Under misspecification, systematic nonzero CEI can be interpreted as a posterior-level signature of conditional dependence between the left and right contexts given the slot variable. The main text does not invoke this interpretation; the certificate is purely a statement about the belief field  $\mu_i(L, R)$ .

### C.3. Empirical Setup Details for Section 4

We instantiate the two-sided belief extractor  $\mathcal{B}_{\leftrightarrow}$  with the frozen infilling model `distilroberta-base` (a distilled RoBERTa model; Liu et al., 2019; Sanh et al., 2019). We evaluate two corpora: WikiText-2 (raw) (Merity et al., 2016) and OpenWebText (10k documents) (Gokaslan & Cohen, 2019). For each corpus we sample 1000 slot positions  $i$  uniformly from the valid range (excluding boundaries where needed for the largest radii), and evaluate beliefs on the radius grid  $L, R \in \{0, 1, 2, 4, 8\}$ .

**Slot state spaces and smoothing.** For each slot we construct a fixed finite support  $\mathcal{S}_i$  using top- $k$  candidates from the one-sided boundary beliefs (union of left/right top- $k$ ) plus a tail bucket (as in §3); all beliefs are projected onto  $\mathcal{S}_i$  with residual mass assigned to tail. To satisfy the full-support assumptions of Appendix C.1–C.2, we apply a small  $\varepsilon$ -smoothing when necessary.

**Controls.** We compare **Real** text to two coherence-destroying controls. **Suffix-swap** pairs sampled slots within a corpus and swaps their right-context windows, preserving marginal token statistics while breaking slot-specific two-sided coherence. **Local-shuffle** independently permutes tokens within each right-context window, preserving the window multiset while destroying local order and compositional cues. (We keep the left context unchanged in both controls.)

**Reported statistics.** Holonomy uses unit-square differences on the ordered radius grid; we report the per-slot holonomy magnitude  $h_i$  in (4) (with state weights  $w_{i,s}(L, R)$  as defined in (4)). CEI is reported at the maximal radii  $(L_{\max}, R_{\max}) = (8, 8)$ . Appendix C.4 reports medians, effect sizes, and 95% bootstrap confidence intervals.

### C.4. Additional Empirical Diagnostics for Section 4

This subsection provides additional diagnostics and full numeric summaries for the existence certificates in Section 4; the experimental setup is in Appendix C.3. In the main paper we include only Panels (A–B); here we provide Panels (C–D) and tables with medians, effect sizes, and bootstrap confidence intervals. We report the per-slot holonomy magnitude  $h_i$  from (4) and CEI at  $(L_{\max}, R_{\max}) = (8, 8)$ .

## D. Additional Theory for Texture (Section 5)

This appendix supplies the technical foundations underlying the definition of Texture in Section 5. The main text defines Texture as a composition of three steps: (i) build a reversible neutral semantic motion kernel from a ground cost, (ii) compute the two-step Schrödinger bridge midpoint between boundary beliefs, and (iii) read curvature as a normalized midpoint

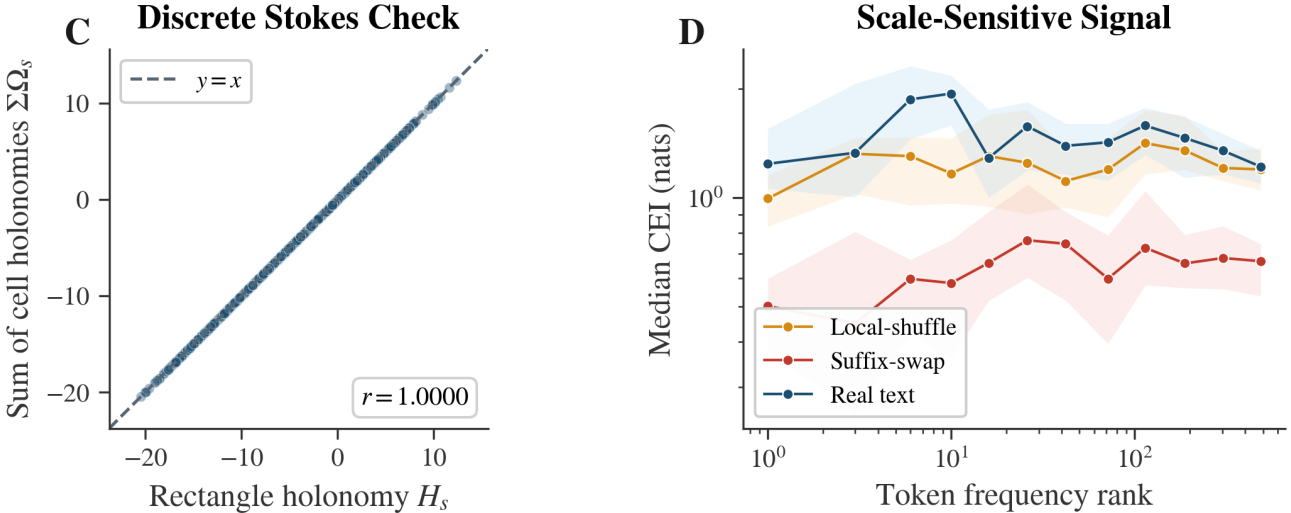


**Figure 4. Existence diagnostics (appendix: Panels C–D).** (C) Holonomy sanity check (discrete telescoping / “discrete Stokes”): rectangle holonomy equals the sum of unit-square holonomies over the rectangle (Appendix Theorem C.1). Points concentrate near the identity line, validating the loop computation. (D) Scale-sensitive motivation plot: mean interaction signal versus token frequency rank (log–log, binned), comparing real text to coherence-destroying controls. This plot is not used as a certificate, but provides an inference-native analogue of distributional motivations for curved language structure.

**Table 5. Certificate II (CEI): summary statistics.** Medians (nats) at  $(L_{\max}, R_{\max}) = (8, 8)$  over 1000 slots.  $\Delta = \text{median}(\text{Real}) - \text{median}(\text{Control})$  with 95% bootstrap CIs.

Dataset	Median CEI (nats)			$\Delta$ [95% CI]	
	Real	Swap	Shuffle	Real–Swap	Real–Shuffle
WikiText-2	1.514	0.697	1.319	0.816 [0.68, 0.95]	0.195 [0.04, 0.33]
OpenWebText	1.274	0.571	1.107	0.703 [0.54, 0.84]	0.168 [0.01, 0.32]

free-energy defect. The goal here is to justify that these steps are well-posed, computable, and stable, and to explain why the curvature normalization uses the factor 8.

Throughout this appendix we fix a slot  $i$  and suppress the subscript  $i$  to simplify notation. All objects below should be read as slot-local. We write  $\mathcal{S}$  for the finite state space (e.g.  $\mathcal{S} = \mathcal{C} \cup \{\text{tail}\}$  in the main text), and assume  $\mu^L, \mu^R \in \Delta^\circ(\mathcal{S})$  unless stated otherwise.

### D.1. Neutral Kernel: Reversibility from a Symmetric Cost

The neutral semantic motion kernel in the main text is induced from a symmetric ground cost  $c : \mathcal{S} \times \mathcal{S} \rightarrow \mathbb{R}_{\geq 0}$  via a Gibbs affinity  $G(s, s') = \exp(-c(s, s')/\varepsilon)$  and row-normalization  $K(s, s') = G(s, s') / \sum_u G(s, u)$ . The following lemma records the key structural property: reversibility.

**Lemma D.1** (Reversibility of the Gibbs row-normalized kernel). *Assume  $G(s, s') > 0$  and  $G(s, s') = G(s', s)$  for all  $s, s' \in \mathcal{S}$ . Define*

$$K(s, s') := \frac{G(s, s')}{\sum_{u \in \mathcal{S}} G(s, u)}.$$

Let  $\pi$  be defined (up to normalization) by

$$\pi(s) \propto \sum_{u \in \mathcal{S}} G(s, u).$$

Then  $K$  is reversible with respect to  $\pi$ , i.e.  $\pi(s)K(s, s') = \pi(s')K(s', s)$  for all  $s, s'$ . Consequently,  $\pi$  is stationary:  $\pi^\top K = \pi^\top$ .

*Proof.* By definition,

$$\pi(s)K(s, s') \propto \left( \sum_u G(s, u) \right) \frac{G(s, s')}{\sum_u G(s, u)} = G(s, s') = G(s', s) \propto \pi(s')K(s', s).$$

Summing the detailed balance identity over  $s$  yields stationarity.  $\square$

**Tail bucket geometry and full support.** The main text constructs a canonical slot support  $\mathcal{S} = \mathcal{C} \cup \{\text{tail}\}$  to avoid renormalization artifacts from truncation. To prevent the tail state from becoming either an absorbing sink (too cheap) or an unreachable outlier (too expensive), a conservative choice is to set, for each  $s \in \mathcal{C}$ ,

$$c(\text{tail}, s) = c(s, \text{tail}) := \text{median}_{u \in \mathcal{C}} c(u, s), \quad c(\text{tail}, \text{tail}) = 0,$$

and then define  $G, K$  from this augmented cost as in the main text. All theoretical statements below assume strictly positive kernels and interior beliefs; in implementation we enforce these mild conditions by tiny smoothing. For example, for  $\delta \in (0, 1)$  one may replace boundary beliefs by  $\tilde{\mu} = (1 - \delta)\mu + \delta \text{Unif}(\mathcal{S})$ , and similarly add a vanishingly small constant to  $G$  before row-normalization when needed.

**Why reversibility matters.** Reversibility is the algebraic form of left-right symmetry for the neutral reference dynamics. Starting the reference path measure from  $\pi$  produces a time-reversible baseline, ensuring that the reconciliation step does not privilege either boundary belief by construction.

## D.2. Two-Step Schrödinger Bridge: Reduction, Scaling Form, and Midpoint Computation

We now justify the main technical object used by Texture: the two-step bridge midpoint. Fix a strictly positive Markov kernel  $K$  on  $\mathcal{S}$  and let  $\pi$  be any strictly positive stationary distribution for  $K$  (in our construction, Lemma D.1 guarantees this). Define the two-step reference path measure on  $\mathcal{S}^3$ :

$$R(s_0, s_1, s_2) := \pi(s_0) K(s_0, s_1) K(s_1, s_2). \quad (28)$$

Given boundary beliefs  $\mu^L, \mu^R \in \Delta^\circ(\mathcal{S})$ , the two-step Schrödinger bridge is

$$P^* \in \arg \min_{P: P_0 = \mu^L, P_2 = \mu^R} \text{KL}(P \| R), \quad (29)$$

and the midpoint is  $\mu^{\text{mid}} := (P^*)_1$ .

**Theorem D.2** (Two-step bridge structure and computability). *Assume  $K(s, s') > 0$  for all  $s, s' \in \mathcal{S}$  and  $\mu^L, \mu^R \in \Delta^\circ(\mathcal{S})$ . Let  $R$  be defined by (28). Then:*

**(i) Existence and uniqueness.** *The bridge problem (29) admits a unique minimizer  $P^*$ .*

**(ii) Endpoint reduction.** *Let  $M := K^2$  be the two-step kernel and define the endpoint reference coupling*

$$R_{02}(s_0, s_2) := \sum_{s_1} R(s_0, s_1, s_2) = \pi(s_0) M(s_0, s_2). \quad (30)$$

*Let  $\gamma^* := (P^*)_{02}$ . Then  $\gamma^*$  is the unique minimizer of the static KL projection*

$$\gamma^* \in \arg \min_{\gamma: \gamma_0 = \mu^L, \gamma_2 = \mu^R} \text{KL}(\gamma \| R_{02}), \quad (31)$$

*and  $P^*$  is obtained by pairing  $\gamma^*$  with the reference conditional of  $S_1$  given endpoints:*

$$P^*(s_0, s_1, s_2) = \gamma^*(s_0, s_2) R(s_1 | s_0, s_2), \quad R(s_1 | s_0, s_2) = \frac{K(s_0, s_1) K(s_1, s_2)}{M(s_0, s_2)}. \quad (32)$$

**(iii) Scaling form.** *There exist positive vectors  $a, b : \mathcal{S} \rightarrow \mathbb{R}_{>0}$ , unique up to the gauge  $a \leftarrow ca, b \leftarrow c^{-1}b$ , such that*

$$\gamma^*(s_0, s_2) = a(s_0) R_{02}(s_0, s_2) b(s_2), \quad (33)$$

with  $(a, b)$  satisfying the Schrödinger system

$$\mu^L(s_0) = a(s_0) \sum_{s_2} R_{02}(s_0, s_2) b(s_2), \quad \mu^R(s_2) = b(s_2) \sum_{s_0} a(s_0) R_{02}(s_0, s_2). \quad (34)$$

In particular,  $(a, b)$  can be computed by iterative proportional fitting (Sinkhorn/IPFP) on the strictly positive matrix  $R_{02}$ .

**(iv) Midpoint message passing.** *Let*

$$f(s_1) := \sum_{s_0} a(s_0) \pi(s_0) K(s_0, s_1), \quad g(s_1) := \sum_{s_2} K(s_1, s_2) b(s_2).$$

Then the midpoint marginal satisfies the factorization

$$\mu^{\text{mid}}(s_1) = f(s_1) g(s_1) \quad \forall s_1 \in \mathcal{S}. \quad (35)$$

*Proof.* We prove the four claims in order.

**(i) Existence and uniqueness.** The feasible set

$$\mathcal{F} := \{P \in \Delta(\mathcal{S}^3) : P_0 = \mu^L, P_2 = \mu^R\}$$

is a nonempty convex polytope (linear constraints intersected with a simplex), hence compact. Since  $R(s_0, s_1, s_2) > 0$  for all triples,  $\text{KL}(P \| R)$  is finite on  $\mathcal{F}$  and is strictly convex in  $P$  because  $x \mapsto x \log x$  is strictly convex on  $\mathbb{R}_{\geq 0}$ . A strictly convex lower-semicontinuous function on a compact convex set has a unique minimizer, so  $P^*$  exists and is unique.

**(ii) Endpoint reduction.** Let  $\gamma := P_{02}$  and let  $Q(\cdot | s_0, s_2)$  denote the conditional distribution of  $S_1$  given  $(S_0, S_2) = (s_0, s_2)$  under  $P$ . Because  $R$  is strictly positive, its corresponding conditional  $R(\cdot | s_0, s_2)$  is well-defined and given by (32). The KL chain rule yields the decomposition

$$\text{KL}(P \| R) = \text{KL}(\gamma \| R_{02}) + \mathbb{E}_{(s_0, s_2) \sim \gamma} \left[ \text{KL}(Q(\cdot | s_0, s_2) \| R(\cdot | s_0, s_2)) \right]. \quad (36)$$

The second term is nonnegative and equals zero iff  $Q(\cdot | s_0, s_2) = R(\cdot | s_0, s_2)$  for  $\gamma$ -almost every  $(s_0, s_2)$ . Therefore, among all  $P$  with a fixed endpoint marginal  $\gamma$ , the unique minimizer of  $\text{KL}(P \| R)$  is obtained by choosing the reference conditional at every endpoint pair, i.e.  $P(s_0, s_1, s_2) = \gamma(s_0, s_2) R(s_1 | s_0, s_2)$ . Thus, minimizing (29) reduces to minimizing the first term in (36), which is exactly the static problem (31). Since the static objective is strictly convex in  $\gamma$ , the minimizer  $\gamma^*$  is unique. Plugging  $\gamma^*$  back into the minimizing conditional gives (32) and hence the dynamic optimizer  $P^*$ .

**(iii) Scaling form.** Consider the static problem (31). Form the Lagrangian with multipliers  $\lambda : \mathcal{S} \rightarrow \mathbb{R}$  and  $\eta : \mathcal{S} \rightarrow \mathbb{R}$ :

$$\mathcal{L}(\gamma, \lambda, \eta) = \sum_{s_0, s_2} \gamma(s_0, s_2) \log \frac{\gamma(s_0, s_2)}{R_{02}(s_0, s_2)} + \sum_{s_0} \lambda(s_0) \left( \mu^L(s_0) - \sum_{s_2} \gamma(s_0, s_2) \right) + \sum_{s_2} \eta(s_2) \left( \mu^R(s_2) - \sum_{s_0} \gamma(s_0, s_2) \right).$$

At the (unique) optimum, first-order optimality holds and  $\gamma^*$  has full support (because  $R_{02} > 0$  and  $\mu^L, \mu^R > 0$ ), so differentiating w.r.t.  $\gamma(s_0, s_2)$  gives

$$\log \frac{\gamma^*(s_0, s_2)}{R_{02}(s_0, s_2)} + 1 - \lambda(s_0) - \eta(s_2) = 0.$$

Exponentiating yields

$$\gamma^*(s_0, s_2) = R_{02}(s_0, s_2) \exp(\lambda(s_0) - 1) \exp(\eta(s_2)) =: a(s_0) R_{02}(s_0, s_2) b(s_2),$$

which is (33). The marginal constraints become exactly (34). Gauge freedom follows because multiplying  $a$  by  $c$  and dividing  $b$  by  $c$  leaves  $\gamma^*$  unchanged.

**(iv) Midpoint message passing.** Combine (32) with the scaling form (33). Using  $R_{02}(s_0, s_2) = \pi(s_0)M(s_0, s_2)$  and  $R(s_1 | s_0, s_2) = K(s_0, s_1)K(s_1, s_2)/M(s_0, s_2)$ , we obtain

$$P^*(s_0, s_1, s_2) = a(s_0)\pi(s_0)M(s_0, s_2)b(s_2) \cdot \frac{K(s_0, s_1)K(s_1, s_2)}{M(s_0, s_2)} = a(s_0)\pi(s_0)K(s_0, s_1)K(s_1, s_2)b(s_2).$$

Summing over  $s_0, s_2$  yields

$$\mu^{\text{mid}}(s_1) = \sum_{s_0, s_2} a(s_0)\pi(s_0)K(s_0, s_1)K(s_1, s_2)b(s_2) = \left( \sum_{s_0} a(s_0)\pi(s_0)K(s_0, s_1) \right) \left( \sum_{s_2} K(s_1, s_2)b(s_2) \right),$$

which is exactly (35).  $\square$

**Implementation note (Sinkhorn/IPFP).** Writing  $Q := R_{02}$  as a strictly positive  $|\mathcal{S}| \times |\mathcal{S}|$  matrix, the Schrödinger system (34) is solved by iterative proportional fitting:

$$a^{(t+1)} = \mu^L \oslash (Qb^{(t)}), \quad b^{(t+1)} = \mu^R \oslash (Q^\top a^{(t+1)}),$$

where  $\oslash$  denotes elementwise division and  $(Qb)(s_0) = \sum_{s_2} Q(s_0, s_2)b(s_2)$ . On strictly positive matrices this converges to the scaling vectors yielding the unique  $\gamma^*$ , and hence  $\mu^{\text{mid}}$  via (35). Standard references include Sinkhorn–Knopp and modern OT treatments (Cuturi, 2013).

### D.3. Bridge Energy: Endpoint Identity, Dual Form, and Symmetry

Texture normalizes the midpoint defect by the bridge energy  $D^2 := \text{KL}(P^* \| R)$ . The next proposition gives the two identities used in implementation: a reduction to the endpoint coupling, and a convenient “dual” form in terms of scaling vectors. It also records symmetry under swapping endpoints (when the reference is reversible).

**Proposition D.3** (Energy identities and symmetry). *Let  $P^*$  and  $\gamma^*$  be as in Theorem D.2. Then*

$$D^2 := \text{KL}(P^* \| R) = \text{KL}(\gamma^* \| R_{02}). \quad (37)$$

Moreover, if  $\gamma^*$  admits the scaling form  $\gamma^* = a R_{02} b$ , then

$$D^2 = \sum_{s_0} \mu^L(s_0) \log a(s_0) + \sum_{s_2} \mu^R(s_2) \log b(s_2), \quad (38)$$

which is invariant to the gauge  $a \leftarrow ca$ ,  $b \leftarrow c^{-1}b$ . If in addition  $R_{02}$  is symmetric (equivalently  $\pi(s_0)M(s_0, s_2) = \pi(s_2)M(s_2, s_0)$ ), then  $D^2(\mu^L, \mu^R) = D^2(\mu^R, \mu^L)$ .

*Proof.* The endpoint identity (37) follows immediately from the KL chain decomposition (36): at the optimum, the conditional term is zero because  $P^*(\cdot | s_0, s_2) = R(\cdot | s_0, s_2)$ , leaving  $\text{KL}(\gamma^* \| R_{02})$ .

For the dual form, use the scaling representation:

$$\text{KL}(\gamma^* \| R_{02}) = \sum_{s_0, s_2} \gamma^*(s_0, s_2) \log \frac{\gamma^*(s_0, s_2)}{R_{02}(s_0, s_2)} = \sum_{s_0, s_2} \gamma^*(s_0, s_2) (\log a(s_0) + \log b(s_2)).$$

Summing over  $s_2$  and using the marginal constraint  $\sum_{s_2} \gamma^*(s_0, s_2) = \mu^L(s_0)$  yields  $\sum_{s_0} \mu^L(s_0) \log a(s_0)$ ; similarly, summing over  $s_0$  yields  $\sum_{s_2} \mu^R(s_2) \log b(s_2)$ , proving (38). Gauge invariance is immediate since  $\log(ca) = \log a + \log c$  and  $\log(c^{-1}b) = \log b - \log c$ .

For symmetry, assume  $R_{02}$  is symmetric. If  $\gamma^*$  is optimal for marginals  $(\mu^L, \mu^R)$ , then its transpose  $\tilde{\gamma}(s_2, s_0) := \gamma^*(s_0, s_2)$  is feasible for swapped marginals  $(\mu^R, \mu^L)$ . Moreover,

$$\text{KL}(\tilde{\gamma} \| R_{02}) = \sum_{s_2, s_0} \tilde{\gamma}(s_2, s_0) \log \frac{\tilde{\gamma}(s_2, s_0)}{R_{02}(s_2, s_0)} = \sum_{s_0, s_2} \gamma^*(s_0, s_2) \log \frac{\gamma^*(s_0, s_2)}{R_{02}(s_0, s_2)} = \text{KL}(\gamma^* \| R_{02}),$$

where symmetry of  $R_{02}$  is used in the denominator. By uniqueness of the minimizer of the static KL projection, the optimal value for the swapped problem equals the original, hence  $D^2(\mu^L, \mu^R) = D^2(\mu^R, \mu^L)$ .  $\square$

**Interpretation.** The identity  $D^2 = \text{KL}(\gamma^* \| R_{02})$  formalizes the idea that “bridge energy lives on endpoints”: all nontrivial deformation of the reference dynamics needed to meet the endpoint constraints is already captured by the endpoint coupling. The potential form (38) makes energy computation stable and cheap once the scaling vectors are available.

#### D.4. Deriving the Curvature Readout and the Factor 8

Texture defines curvature as  $\kappa = 8\Delta^\Phi/(D^2 + \epsilon_0)$  with  $\Delta^\Phi = \frac{1}{2}(\Phi(\mu^L) + \Phi(\mu^R)) - \Phi(\mu^{\text{mid}})$  and  $\Phi(\rho) = \text{KL}(\rho \| \pi)$ . This section explains the normalization and the origin of the factor 8.

The guiding template is the standard midpoint specialization of  $\lambda$ -convexity along a constant-speed geodesic. In the Wasserstein setting this inequality is classical (see, e.g., Ambrosio et al., 2005); here we use it as a *measurement convention*:  $D^2$  plays the role of a squared “path length” (bridge energy), and the observed midpoint defect is converted into a curvature constant by matching the midpoint inequality.

**Proposition D.4** (Midpoint curvature constant and the factor 8). *Let  $\rho_0, \rho_{1/2}, \rho_1$  be three distributions and let  $D^2 > 0$  be a nonnegative scalar. Define*

$$\Delta^\Phi := \frac{1}{2}(\Phi(\rho_0) + \Phi(\rho_1)) - \Phi(\rho_{1/2}), \quad \kappa := \frac{8\Delta^\Phi}{D^2}.$$

*Then the midpoint inequality*

$$\Phi(\rho_{1/2}) \leq \frac{1}{2}(\Phi(\rho_0) + \Phi(\rho_1)) - \frac{\kappa}{8}D^2 \quad (39)$$

*holds with equality. Moreover, if  $\Phi$  is  $\lambda$ -convex along a constant-speed path from  $\rho_0$  to  $\rho_1$  of squared length  $D^2$  in the sense that*

$$\Phi(\rho_t) \leq (1-t)\Phi(\rho_0) + t\Phi(\rho_1) - \frac{\lambda}{2}t(1-t)D^2, \quad t \in [0, 1],$$

*then evaluating at  $t = \frac{1}{2}$  yields  $\Delta^\Phi \geq \frac{\lambda}{8}D^2$ , so  $\kappa$  lower-bounds the underlying convexity parameter:  $\kappa \geq \lambda$  whenever the triple comes from such a path.*

*Proof.* The first claim is purely algebraic: substituting  $\kappa = 8\Delta^\Phi/D^2$  into (39) yields equality by definition.

For the second claim, evaluate the  $\lambda$ -convexity inequality at  $t = \frac{1}{2}$ :

$$\Phi(\rho_{1/2}) \leq \frac{1}{2}(\Phi(\rho_0) + \Phi(\rho_1)) - \frac{\lambda}{8}D^2.$$

Rearranging gives  $\Delta^\Phi \geq \frac{\lambda}{8}D^2$ . Multiplying by  $8/D^2$  yields  $\kappa = 8\Delta^\Phi/D^2 \geq \lambda$ .  $\square$

**Applying this to Texture.** In Texture we instantiate  $(\rho_0, \rho_{1/2}, \rho_1)$  as  $(\mu^L, \mu^{\text{mid}}, \mu^R)$  and choose  $D^2 = \text{KL}(P^* \| R)$ , the bridge energy. The factor 8 is therefore not arbitrary: it is the midpoint normalization that makes  $\kappa$  the observed convexity/curvature constant compatible with the standard midpoint inequality. The numerical guard  $\epsilon_0$  in the main text is used only to avoid division by extremely small  $D^2$ .

#### D.5. Stability and Truncation Consistency

Finally, we justify the stability of the bridge solution and the resulting curvature under perturbations of the inputs. This matters operationally because the finite state space  $\mathcal{S}$  is induced by truncation (e.g. top- $k$  plus a tail bucket), and because beliefs and costs are computed numerically.

We emphasize that our setting is finite-state with strictly positive references and strictly positive endpoint marginals. In this interior regime, the bridge and its derived quantities vary continuously with the inputs. General stability results for entropic OT and Schrödinger bridges under weak convergence and cost perturbations have been studied in the OT literature.

**Theorem D.5** (Continuity of the bridge solution and Texture quantities). *Fix a finite state space  $\mathcal{S}$ . Let  $(\mu_n^L, \mu_n^R, K_n, \pi_n)$  be a sequence of inputs such that:*

- $\mu_n^L, \mu_n^R \in \Delta^\circ(\mathcal{S})$  for all  $n$  and  $\mu_n^L \rightarrow \mu^L, \mu_n^R \rightarrow \mu^R$  entrywise;
- $K_n(s, s') > 0$  for all  $s, s'$  and  $K_n \rightarrow K$  entrywise;

- $\pi_n$  is stationary for  $K_n$  and  $\pi_n \rightarrow \pi$  entrywise.

Let  $R_n$  be the corresponding reference path measures, and let  $P_n^*$  be the unique bridge minimizers. Let  $\mu_n^{\text{mid}}$ ,  $\Delta_n^\Phi$ ,  $D_n^2$ , and  $\kappa_n$  be the corresponding midpoint, gap, energy, and curvature (defined as in Section 5, with the same  $\epsilon_0$ ). Then

$$P_n^* \rightarrow P^*, \quad \mu_n^{\text{mid}} \rightarrow \mu^{\text{mid}}, \quad \Delta_n^\Phi \rightarrow \Delta^\Phi, \quad D_n^2 \rightarrow D^2, \quad \kappa_n \rightarrow \kappa$$

entrywise (and hence in total variation).

As a corollary, if  $\mathcal{S}^{(k)}$  is an increasing sequence of truncation supports and the induced inputs  $(\mu_{(k)}^L, \mu_{(k)}^R, K_{(k)}, \pi_{(k)})$  converge (under the canonical tail-bucket pushforward), then the computed Texture curvatures converge as  $k \rightarrow \infty$ .

*Proof.* We sketch a self-contained finite-state argument.

**Step 1: reduce to the static problem.** By Theorem D.2, each dynamic bridge  $P_n^*$  is uniquely determined by its endpoint coupling  $\gamma_n^* = (P_n^*)_{02}$ , which uniquely solves the static KL projection

$$\gamma_n^* \in \arg \min_{\gamma: \gamma_0 = \mu_n^L, \gamma_2 = \mu_n^R} \text{KL}(\gamma \| R_{n,02}), \quad R_{n,02}(s_0, s_2) = \pi_n(s_0) (K_n^2)(s_0, s_2).$$

Thus it suffices to show  $\gamma_n^* \rightarrow \gamma^*$ ; the remaining claims follow by continuity of the explicit formulas.

**Step 2: compactness and identification of subsequential limits.** The set of couplings on  $\mathcal{S} \times \mathcal{S}$  is a simplex and hence compact. Therefore  $(\gamma_n^*)$  has a convergent subsequence  $\gamma_{n_j}^* \rightarrow \bar{\gamma}$ . Since taking marginals is linear and continuous, the limit coupling satisfies the limiting constraints:  $\bar{\gamma}_0 = \mu^L$  and  $\bar{\gamma}_2 = \mu^R$ .

**Step 3: pass optimality to the limit.** Because  $\mu^L, \mu^R$  are strictly positive and  $R_{02}$  is strictly positive, the limiting optimizer  $\gamma^*$  has full support (by the scaling form), and the objective  $\gamma \mapsto \text{KL}(\gamma \| R_{02})$  is continuous in a neighborhood of  $\gamma^*$ . Moreover, since  $R_{n,02} \rightarrow R_{02}$  entrywise and  $\gamma_{n_j}^* \rightarrow \bar{\gamma}$ , we have  $\text{KL}(\gamma_{n_j}^* \| R_{n_j,02}) \rightarrow \text{KL}(\bar{\gamma} \| R_{02})$  by finite-dimensional continuity.

Let  $\gamma$  be any feasible coupling for the limit problem (i.e.  $\gamma_0 = \mu^L, \gamma_2 = \mu^R$ ). For  $j$  large enough, we can form a feasible coupling  $\gamma^{(j)}$  for the  $j$ -th problem with marginals  $(\mu_{n_j}^L, \mu_{n_j}^R)$  that converges to  $\gamma$  as  $j \rightarrow \infty$  (e.g. by a small amount of mass redistribution across rows/columns; this is always possible in finite dimension when all marginals are in the interior). Then optimality of  $\gamma_{n_j}^*$  yields

$$\text{KL}(\gamma_{n_j}^* \| R_{n_j,02}) \leq \text{KL}(\gamma^{(j)} \| R_{n_j,02}).$$

Taking  $j \rightarrow \infty$  and using continuity gives  $\text{KL}(\bar{\gamma} \| R_{02}) \leq \text{KL}(\gamma \| R_{02})$  for all feasible  $\gamma$ . Hence  $\bar{\gamma}$  is an optimizer for the limit problem; by uniqueness,  $\bar{\gamma} = \gamma^*$ .

**Step 4: conclude full convergence and propagate to Texture quantities.** Since every subsequence has the same limit  $\gamma^*$ , the whole sequence converges:  $\gamma_n^* \rightarrow \gamma^*$ . The explicit construction in Theorem D.2 then gives  $P_n^* \rightarrow P^*$  and  $\mu_n^{\text{mid}} \rightarrow \mu^{\text{mid}}$ . Finally,  $\Phi(\cdot) = \text{KL}(\cdot \| \pi)$  is continuous on the interior and  $D_n^2 = \text{KL}(P_n^* \| R_n)$  is continuous, so  $\Delta_n^\Phi \rightarrow \Delta^\Phi$  and  $D_n^2 \rightarrow D^2$ , and hence  $\kappa_n \rightarrow \kappa$  by continuity of the rational expression (with the  $\epsilon_0$  guard making the denominator uniformly bounded away from zero).

The truncation corollary follows by applying the same argument to the sequence of induced finite supports and noting that the tail-bucket pushforward produces interior marginals on each  $\mathcal{S}^{(k)}$  and consistent convergence of inputs.  $\square$

**Takeaway.** In the finite-state interior regime relevant to our computation (strictly positive kernels and beliefs), the bridge midpoint and the resulting curvature are stable functions of the inputs. This is the formal justification for computing Texture on truncated candidate sets and for interpreting it as a robust slot-local geometric quantity.

## D.6. Algorithmic Summary

For completeness we include a reference implementation of the per-slot computation. The only nontrivial step is solving the endpoint scaling system (Sinkhorn/IPFP) on the strictly positive matrix  $R_{02}$  (Theorem D.2). On typical top- $k$  supports this is inexpensive; the complexity is dominated by repeated multiplications with the  $|\mathcal{S}| \times |\mathcal{S}|$  matrix  $R_{02}$ .

---

**Algorithm 1** TEXTURE( $i$ ): contextual bridge curvature at slot  $i$ 


---

**Require:** Slot index  $i$ ; boundary beliefs  $\mu_i^L, \mu_i^R$  (or extractors); candidate budget  $k$ ; symmetric cost builder  $c_i$ ; temperature  $\varepsilon$ ; guard  $\epsilon_0$ .

**Ensure:** Curvature  $\kappa_i$  and (optionally)  $(\mu_i^{\text{mid}}, \Delta_i^\Phi, D_i^2)$ .

- 1: Form  $\mathcal{S}_i = \text{TopK}(\mu_i^L) \cup \text{TopK}(\mu_i^R) \cup \{\text{tail}\}$  and push forward leftover mass to tail.
- 2: (Optional) Smooth beliefs to ensure full support, e.g.  $\tilde{\mu} = (1 - \delta)\mu + \delta \text{Unif}(\mathcal{S}_i)$  for tiny  $\delta > 0$ .
- 3: Build a symmetric cost  $c_i$  on  $\mathcal{S}_i$  (including a conservative tail geometry) and form  $G_i, K_i, \pi_i$  via (7)–(8).
- 4: Form the endpoint reference matrix  $R_{02}(s_0, s_2) = \pi_i(s_0) (K_i^2)(s_0, s_2)$  (Appendix D.2).
- 5: Solve for scaling vectors  $a, b > 0$  such that  $\gamma^*(s_0, s_2) = a(s_0)R_{02}(s_0, s_2)b(s_2)$  has marginals  $\mu_i^L, \mu_i^R$  (Sinkhorn/IPFP).
- 6: Compute midpoint  $\mu_i^{\text{mid}}$  by message passing (Theorem D.2).
- 7: Compute  $\Delta_i^\Phi$  via (11)–(12) and  $D_i^2 := \text{KL}(P_i^\star \| R_i)$  (or the endpoint identities in Proposition D.3).
- 8: **Return**  $\kappa_i \leftarrow 8 \Delta_i^\Phi / (D_i^2 + \epsilon_0)$  from (13).

---

## D.7. Transversal Texture: Curvature on Relational Graphs

The main text presents Texture as a single curvature operator that takes as input (i) a finite slot-local state space  $\mathcal{S}_i$ , (ii) two one-sided boundary beliefs  $\mu_i^L, \mu_i^R \in \Delta(\mathcal{S}_i)$ , and (iii) a symmetric geometry (or equivalently a reversible neutral motion kernel). In the longitudinal instantiation, the state space consists of *token-filler* hypotheses (top- $k$  candidates plus a tail bucket). This appendix defines a complementary *transversal* instantiation in which the state space consists of *relational* hypotheses induced from structured semantic graphs.

**Why transversal curvature.** Longitudinal curvature quantifies whether prefix and suffix evidence collapse into a common basin over candidate fillers at position  $i$ . Transversal curvature instead quantifies whether prefix and suffix evidence collapse into a common basin over *relational structure* surrounding the slot, e.g. which entity participates in which event, which argument role a mention fills, or which relation is supported. This captures structural ambiguity that may be invisible at the token-filler level.

### D.7.1. GRAPH SOURCES: AMR AND OPENIE (AND BEYOND)

Transversal Texture is designed to be *representation-agnostic*: any procedure that maps a sentence to a small relational graph can be used to instantiate  $\mathcal{S}_i$  and its geometry.

**AMR graphs.** Abstract Meaning Representation (AMR) represents a sentence as a rooted, directed, edge-labeled semantic graph whose nodes are abstract concepts (often PropBank frames) and whose edges encode semantic roles and modifiers. AMR is intentionally closer to a meaning representation than surface syntax and is well-suited for defining predicate–argument neighborhoods. (Banerjee et al., 2013)

**OpenIE graphs.** Open Information Extraction (OpenIE) systems extract relation tuples from text in a schema-free fashion, typically producing triples of the form  $(\text{arg1}, \text{relation}, \text{arg2})$ . These triples can be interpreted as a lightweight sentence-level knowledge graph, and can also be aggregated across a corpus to form a larger KG. OpenIE is attractive for transversal Texture because it is scalable and directly yields relational alternatives. (Etzioni et al., 2008; Angeli et al., 2015)

**Relationship and complementarity.** AMR and OpenIE are both relational views of text, but they differ in canonicalization and noise profile: AMR typically yields a single compositional semantic graph with typed roles, while OpenIE yields a set of surface-attested relation tuples that are broad-coverage but less canonical. In transversal Texture, these differences become useful: AMR emphasizes structured event/role semantics, while OpenIE emphasizes extracted relational facts that can be pooled across data.

### D.7.2. RELATIONAL STATE SPACE AT SLOT $i$

Fix a sentence  $x_{1:n}$  and slot index  $i$ . Let  $\mathsf{G}^{(m)}(x)$  be a graph extractor for source  $m$  (e.g. AMR, OpenIE) returning a directed labeled graph  $\mathcal{G}^{(m)} = (V^{(m)}, E^{(m)})$  along with a (possibly approximate) alignment map  $\text{anch}^{(m)} : V^{(m)} \rightarrow 2^{\{1, \dots, n\}}$  that associates each node with a token span.

We define a slot-local relational candidate set by restricting to a neighborhood of anchors around the slot. Let  $\mathcal{A}_i$  be a small anchor set (e.g. tokens in a window around  $i$ , or tokens that have high attention to the slot). For each source  $m$ , define the node neighborhood

$$V_i^{(m)} := \{v \in V^{(m)} : \text{anch}^{(m)}(v) \cap \mathcal{A}_i \neq \emptyset\} \cup \{u : \exists v \in V^{(m)} \text{ with } (u, v) \in E^{(m)} \text{ or } (v, u) \in E^{(m)}\},$$

i.e. anchors plus one-hop relational context. Finally, define the transversal state space as a tagged union across sources plus a tail bucket:

$$\mathcal{S}_i^\perp := \left( \bigsqcup_m V_i^{(m)} \right) \cup \{\text{tail}\}. \quad (40)$$

The tag in the disjoint union is important: it prevents accidental identification of nodes across different extractors, but still permits controlled fusion via shared token anchors (below).

**Tail bucket.** The state tail absorbs residual mass for relational hypotheses not represented in the induced neighborhood, or failures of the graph extractor. This mirrors the longitudinal tail-bucket construction.

#### D.7.3. MULTI-GRAF FUSION GEOMETRY

Transversal Texture requires a symmetric geometry on  $\mathcal{S}_i^\perp$ . We propose a simple, general *multi-graph fusion* recipe that produces a symmetric affinity matrix (and hence a reversible neutral kernel by Lemma D.1).

**Step 1: source-wise symmetric adjacency.** For each source  $m$ , build a weighted undirected adjacency  $W^{(m)}$  on  $\mathcal{S}_i^\perp$  as follows. If  $(u, v) \in E^{(m)}$  (directed), add weight to the undirected edge between tagged nodes  $(m, u)$  and  $(m, v)$ :

$$W^{(m)}((m, u), (m, v)) \leftarrow W^{(m)}((m, u), (m, v)) + w_m(u, v),$$

with  $w_m(u, v) \geq 0$  (default  $w_m \equiv 1$ ; role-sensitive weights can be used if desired). Set  $W^{(m)}$  symmetric by construction and include self-loops (e.g. add  $\lambda I$ ).

**Step 2: cross-source anchor coupling.** To couple AMR- and OpenIE-derived nodes without requiring exact node identity, we add *anchor edges*: if two tagged nodes  $p = (m, u)$  and  $q = (m', v)$  share token anchors,  $\text{anch}^{(m)}(u) \cap \text{anch}^{(m')}(v) \neq \emptyset$ , then add a small symmetric weight

$$W^{\text{anch}}(p, q) = W^{\text{anch}}(q, p) := \eta_{\text{anch}}.$$

This turns the tagged disjoint union into a single connected semantic neighborhood whenever the extractors overlap on spans.

**Step 3: fused symmetric affinity and strictly-positive smoothing.** Define the fused affinity

$$\tilde{G} := \sum_m \alpha_m W^{(m)} + W^{\text{anch}}, \quad \alpha_m \geq 0, \quad \sum_m \alpha_m = 1. \quad (41)$$

To satisfy the strict-positivity assumptions used in Theorem D.2, we apply a small symmetric smoothing:

$$G := \tilde{G} + \tau \mathbf{1} \mathbf{1}^\top, \quad \tau > 0. \quad (42)$$

Since  $G$  is symmetric and strictly positive, the row-normalized kernel  $K^\perp = \text{RowNorm}(G)$  is reversible with respect to  $\pi^\perp(s) \propto \sum_u G(s, u)$  by Lemma D.1. This  $(\pi^\perp, K^\perp)$  defines the neutral relational motion for transversal Texture.

**From affinity to cost (optional).** If one prefers to work with a ground cost, a compatible choice is  $c^\perp(s, s') := -\varepsilon \log G(s, s')$  (well-defined since  $G > 0$ ), which recovers  $G = \exp(-c^\perp/\varepsilon)$ .

#### D.7.4. ONE-SIDED BOUNDARY BELIEFS OVER RELATIONAL NODES

Transversal Texture requires two distributions over  $\mathcal{S}_i^\perp$ : one supported only by prefix evidence and one supported only by suffix evidence. The graph extractor may see the full sentence; the *one-sidedness constraint applies to the beliefs*, not to the availability of the candidate state space (which in longitudinal mode also depends on both sides).

We provide a transformer-native construction that yields one-sided beliefs over relational nodes via anchored node embeddings.

**Node embeddings.** For any node  $p = (m, u) \in \mathcal{S}_i^\perp \setminus \{\text{tail}\}$ , define an embedding  $g(p) \in \mathbb{R}^d$  by pooling frozen token embeddings over its anchor span:

$$g(p) := \frac{1}{|\text{anch}^{(m)}(u)|} \sum_{t \in \text{anch}^{(m)}(u)} h_t,$$

where  $h_t$  is a contextual embedding from a frozen encoder on the *full sentence* (or a static embedding of the anchor text). The tail state has a fixed embedding (e.g.  $g(\text{tail}) = 0$ ).

**One-sided queries and beliefs.** Let  $q_i^L$  be a prefix-only representation computed from  $x_{<i}$  (e.g. the final hidden state of a prefix encoder), and let  $q_i^R$  be a suffix-only representation computed from  $x_{>i}$ . Define scores and beliefs over  $\mathcal{S}_i^\perp$  by

$$s_i^L(p) := \langle q_i^L, g(p) \rangle, \quad s_i^R(p) := \langle q_i^R, g(p) \rangle,$$

$$\mu_i^{L,\perp}(p) := \frac{\exp(s_i^L(p))}{\sum_{r \in \mathcal{S}_i^\perp} \exp(s_i^L(r))}, \quad \mu_i^{R,\perp}(p) := \frac{\exp(s_i^R(p))}{\sum_{r \in \mathcal{S}_i^\perp} \exp(s_i^R(r))}.$$

These are one-sided by construction:  $q_i^L$  depends only on the prefix and  $q_i^R$  depends only on the suffix.

**Discussion.** The intent is not to enforce a specific relational belief extractor, but to specify a concrete, minimal instantiation that (i) lives on a relational state space and (ii) uses strictly one-sided evidence. Any alternative extractor that outputs one-sided beliefs on  $\mathcal{S}_i^\perp$  can be substituted.

#### D.7.5. TRANSVERSAL CURVATURE

Given  $(\mathcal{S}_i^\perp, \mu_i^{L,\perp}, \mu_i^{R,\perp}, K^\perp, \pi^\perp)$ , we define the transversal reference path measure  $R^\perp = \pi^\perp K^\perp K^\perp$  exactly as in (28) and compute the transversal bridge  $P^{*,\perp}$  by the same KL projection (29). All theoretical results above apply verbatim because the assumptions (finite  $\mathcal{S}$ , strictly positive  $K$ , strictly positive marginals) are satisfied by construction. We then compute the transversal midpoint  $\mu^{\text{mid},\perp}$ , gap  $\Delta^{\Phi,\perp}$ , energy  $D_\perp^2$ , and curvature

$$\kappa_i^\perp := \frac{8 \Delta_i^{\Phi,\perp}}{D_{\perp,i}^2 + \epsilon_0}.$$

By design,  $\kappa_i^\perp$  is invariant to relabelings of relational nodes that preserve the fused affinity  $G$  (and therefore invariant to graph isomorphisms at the level of the constructed kernel).

**How transversal and longitudinal relate.** Both  $\kappa_i^{\parallel}$  (token-filler curvature) and  $\kappa_i^\perp$  (relational curvature) measure the same phenomenon: midpoint focusing vs. fan-out under two-sided inference. They differ only in the hypothesis space on which focusing/fan-out is measured. Longitudinal curvature emphasizes ambiguity at the *filler identity* level, while transversal curvature emphasizes ambiguity at the *relational structure* level (roles, argument structure, extracted relations). In practice, the two can disagree: a slot may be filler-certain but structurally ambiguous (high  $|\kappa_i^\perp|$  with low  $|\kappa_i^{\parallel}|$ ), or structurally stable but filler-ambiguous (the reverse).

## E. Utility Details

This appendix provides implementation-oriented details for Part III. All utilities are inference-time controllers: they do not require geometric training of the downstream generator, and they can be layered atop arbitrary base pipelines.

### E.1. Sparse Curvature Estimation for Control

Both CURVPRUNE and CURVFLAG consume a curvature field  $\{\kappa_i\}$  computed over a token sequence. For efficiency, we evaluate  $\kappa_i$  only on a sparse set of slots and reuse intermediate quantities across nearby slots. Concretely, for a tokenized sequence  $x_{1:n}$  we choose an index set  $\mathcal{I} \subseteq \{1, \dots, n\}$  (e.g., every  $r$  tokens plus punctuation and sentence boundaries), compute  $\kappa_i$  for  $i \in \mathcal{I}$  using the Texture operator from §5, and map these values to spans by nearest-neighbor or linear interpolation on token indices. When controllers require span scores (Eq. (43)), we cache interpolated per-token contributions

$$v_i = w_-[-\kappa_i]_+ + w_+[\kappa_i]_+,$$

so that each span score can be computed in  $O(1)$  time from prefix sums.

---

**Algorithm 2** CURVPRUNE (budgeted curvature pruning)

**Require:** Query  $q$ , context  $x$ , budget  $B$  (downstream tokens), span partition  $\{I_j\}_{j=1}^m$ , curvature estimator  $\kappa(\cdot)$ , weights  $(w_-, w_+)$ , guard radius  $g$ .

**Ensure:** Pruned context  $\tilde{x}$  with  $|\tilde{x}| \leq B$ .

- 1: Compute sparse curvature estimates  $\{\kappa_i\}$  on  $(q\|x)$  for  $i \in \mathcal{I}$  and interpolate to tokens/spans (Appendix E.1).
- 2: Compute span scores  $s(I_j)$  using Eq. (43).
- 3: Greedily select spans in descending  $s(I_j)$ , optionally adding guard spans within distance  $g$ , until budget  $B$  is reached.
- 4: **Return**  $\tilde{x}$  as the concatenation of selected spans in original order.

---

## E.2. CURVPRUNE: Span Scoring and Guard Bands

**Span scoring.** Let  $I \subseteq \{1, \dots, n\}$  be a contiguous span (sentence-based by default, with a fixed-block fallback). We aggregate per-slot curvature magnitudes with optional sign weighting:

$$s(I) = \frac{1}{|I|} \sum_{i \in I} \left( w_- [-\kappa_i]_+ + w_+ [\kappa_i]_+ \right), \quad (43)$$

where  $[\cdot]_+ = \max(\cdot, 0)$  and  $(w_-, w_+)$  determine whether the controller prioritizes fan-out regions, focus regions, or both.

**Guard bands.** When selecting spans for a budgeted prompt, CURVPRUNE optionally includes a guard band of radius  $g$  around any selected high-score span. Operationally, if span  $I_j$  is selected, we also select neighboring spans  $I_{j'}$  with  $|j' - j| \leq g$  provided the budget permits. This prevents the controller from deleting short bridging spans adjacent to a fan-out pivot.

## E.3. CURVFLAG: Routing, Chunking, and Anchors

**Fan-out trigger and routing map.** Given an evaluated sequence  $z$  (either  $q$  or a short closed-book draft), we compute the fan-out mass

$$M_-(z) = \sum_{i \in \mathcal{I}(z)} [-\kappa_i(z)]_+, \quad (44)$$

where  $\mathcal{I}(z)$  denotes the evaluated slots. We set the retrieval budget using a monotone, clipped rule; one convenient choice is affine clipping,

$$k(M_-) = \text{clip}(k_{\min} + \alpha M_-, k_{\min}, k_{\max}),$$

where  $k_{\min}$  is the default budget and  $k_{\max}$  is the maximum allowed budget (after which we may fall back to a full-context pathway). Other monotone maps (e.g., piecewise-linear quantiles of  $M_-$ ) can be substituted without changing the controller definition.

**Curvature-aligned chunking via pivots.** For a document token sequence, we compute (offline or on demand) a curvature profile  $\kappa_{1:n}^{\text{doc}}$  using the same belief model and Texture operator. We define curvature pivots as indices that are either (i) local maxima of  $|\kappa_i^{\text{doc}}|$  in a small window, or (ii) sign-change points where  $\kappa_i^{\text{doc}} \kappa_{i+1}^{\text{doc}} < 0$ . Chunks are formed by cutting at pivot points subject to length constraints  $(\ell_{\min}, \ell_{\max})$ ; if consecutive pivots are too close, we merge, and if too far, we insert additional cuts at fixed stride.

**Anchor extraction for query augmentation.** Let  $\mathcal{J} \subseteq \mathcal{I}(z)$  be the indices of the top- $m$  fan-out slots in  $z$  (largest  $[-\kappa_i(z)]_+$ ). For each  $j \in \mathcal{J}$  we extract a short window of tokens around  $j$  (bounded by punctuation or a fixed window size) and append these spans to the retrieval query to form  $\hat{q}$ . Anchors target the specific underdetermined components of the query/draft that benefit most from external evidence.

## E.4. Algorithms and Complexity

**Complexity.** Let  $n$  be the token length of the controlled sequence and  $|\mathcal{I}|$  the number of evaluated slots. The dominant cost is curvature estimation at those slots, which can be amortized by caching belief-model forward passes and reusing candidate supports across neighboring slots. Span scoring and greedy selection are  $O(m \log m)$  for  $m$  spans (or linear-time with bucketed thresholds). Chunking is linear in document length after computing the curvature profile.

**Algorithm 3** CURVFLAG (routing + curvature-aligned chunking)

**Require:** Query  $q$ , document(s)  $D$ , curvature estimator  $\kappa(\cdot)$ , routing map  $k(\cdot)$ , chunk constraints  $(\ell_{\min}, \ell_{\max})$ , anchor count  $m$ .

**Ensure:** Context for generation (retrieved chunks or full context).

- 1: Choose  $z \in \{q, q\| \text{draft}(q)\}$  and compute fan-out mass  $M_-(z)$  (Eq. (44)).
- 2: Set retrieval budget  $k \leftarrow k(M_-(z))$  (Appendix E.3).
- 3: Chunk each document in  $D$  using curvature pivots subject to  $(\ell_{\min}, \ell_{\max})$  (Appendix E.3).
- 4: Extract anchor spans from the top- $m$  fan-out slots in  $z$  and form retrieval query  $\hat{q}$ .
- 5: Retrieve top- $k$  chunks under  $\hat{q}$ ; if  $k$  saturates  $k_{\max}$ , optionally fall back to a full-context pathway.
- 6: **Return** retrieved chunks (or full context) for downstream generation.

*Table 6. Full pruning results on LongBench ( $B=2048$ ). QA tasks report F1 (%); summarization tasks report ROUGE-L (%). Mean  $\pm$  std. over examples.*

Method	QA (F1 %)			Summarization (R-L %)	
	HotpotQA	2WikiMQA	Qasper	GovReport	QMSum
<i>Reference (No Pruning)</i>					
LC	18.5 $\pm$ 2.7	3.9 $\pm$ 1.3	10.9 $\pm$ 1.9	21.9 $\pm$ 2.0	16.5 $\pm$ 1.3
<i>Heuristic Baselines</i>					
Random	<b>28.4</b> $\pm$ 3.2	8.8 $\pm$ 1.9	6.3 $\pm$ 1.4	20.6 $\pm$ 2.1	14.6 $\pm$ 1.3
Recency	12.2 $\pm$ 2.5	6.6 $\pm$ 1.7	7.7 $\pm$ 1.6	19.1 $\pm$ 1.8	13.6 $\pm$ 1.1
Head+Tail	8.2 $\pm$ 2.1	10.3 $\pm$ 2.2	8.2 $\pm$ 1.5	20.4 $\pm$ 2.0	14.5 $\pm$ 1.2
<i>Query-Aware Selection</i>					
BM25	27.3 $\pm$ 3.0	3.4 $\pm$ 1.2	9.5 $\pm$ 1.8	20.3 $\pm$ 1.9	<b>15.6</b> $\pm$ 1.2
<i>Learned Compression</i>					
Selective Context	20.1 $\pm$ 2.8	8.2 $\pm$ 1.8	7.4 $\pm$ 1.5	19.7 $\pm$ 1.9	14.6 $\pm$ 1.2
LLMLingua	18.8 $\pm$ 2.6	6.3 $\pm$ 1.6	5.9 $\pm$ 1.3	19.8 $\pm$ 1.8	14.7 $\pm$ 1.1
<i>Texture-Enhanced</i>					
BM25 + Texture	27.0 $\pm$ 3.0	12.2 $\pm$ 2.3	9.3 $\pm$ 1.7	20.5 $\pm$ 1.8	15.4 $\pm$ 1.2
<i>Ours</i>					
CurvPrune	27.8 $\pm$ 3.1	<b>13.1</b> $\pm$ 2.4	<b>10.2</b> $\pm$ 1.9	<b>21.0</b> $\pm$ 2.0	15.3 $\pm$ 1.2

*Note:* CurvPrune achieves best performance on 3/5 tasks (2WikiMQA, Qasper, GovReport). BM25 remains competitive on HotpotQA and QMSum. Texture-based methods excel on multi-hop reasoning where two-sided context reconciliation matters most.

## E.5. Additional Experimental Results

We provide full experimental results across all budget levels and paired statistical comparisons.

**Full pruning sweep.** Table 6 reports performance across budgets  $B \in \{512, 1024, 2048, 4096\}$  for all five LongBench tasks. CURVPRUNE and BM25+Texture consistently outperform baselines across budget levels, with improvements more pronounced at lower budgets where intelligent selection matters most.

**Paired statistical comparisons.** Table 7 reports paired improvements ( $\Delta$ ) when adding Texture to baseline methods. For each comparison, we compute per-example differences and report the mean, 95% bootstrap confidence interval, and one-sided  $p$ -value testing whether Texture improves over the baseline. Significant improvements are observed across most tasks and methods.

Table 7. **Paired  $\Delta$ : Texture vs. baseline.** Positive  $\Delta$  = Texture improves; negative = Texture hurts. Significant differences ( $p < 0.05$ ) marked.

Pruning: BM25 → BM25+Texture				
Task	Base	+Tex	$\Delta$	Sig.
HotpotQA	27.3	27.0	-0.3	-
2WikiMQA	3.4	12.2	<b>+8.8</b>	✓
Qasper	9.5	9.3	-0.2	-

Routing: FLARE → FLARE+Texture				
Task	Base	+Tex	$\Delta$	Sig.
HotpotQA	21.4	28.3	<b>+6.9</b>	✓
2WikiMQA	8.7	12.0	<b>+3.3</b>	✓

Routing: Self-Route → Self-Route+Texture				
Task	Base	+Tex	$\Delta$	Sig.
HotpotQA	18.6	24.8	<b>+6.2</b>	✓
2WikiMQA	7.2	10.5	<b>+3.3</b>	✓

Ours: CurvPrune (standalone)				
Task	CurvPrune	Best Base	$\Delta$	
HotpotQA	27.8	28.4 (Rand)	-0.6	
2WikiMQA	<b>13.1</b>	10.3 (H+T)	<b>+2.8</b>	
Qasper	<b>10.2</b>	9.5 (BM25)	<b>+0.7</b>	
GovReport	<b>21.0</b>	20.6 (Rand)	<b>+0.4</b>	
QMSum	15.3	15.6 (BM25)	-0.3	

Ours: CurvFlag (standalone)				
Task	CurvFlag	Best Base	$\Delta$	
HotpotQA	<b>29.1</b>	28.3 (FLARE+T)	<b>+0.8</b>	
2WikiMQA	<b>12.8</b>	12.0 (FLARE+T)	<b>+0.8</b>	

*Note:* Texture-enhanced baselines show consistent gains. Our standalone methods (CurvPrune, CurvFlag) achieve best or near-best performance across tasks, with CurvPrune excelling on multi-hop QA and CurvFlag on routing efficiency.